UNIVERSITAT POLITÈCNICA DE CATALUNYA
BARCELONATECH
Escola d'Enginyeria de Barcelona Est

B.Sc. DISSERTATION

Bachelor's degree in Mechanical Engineering

DESIGN OF A COOLING SYSTEM OF AN ELECTRIC FORMULA STUDENT CAR

Memory and Annexes

Author: Luis Alberto Castrillo Jiménez
Director: Alfredo Guardo Zabaleta
Summons: October 2018

Resum

La incorporació d'un sistema al tren de potència de motor a roda per un vehicle de Formula Student requereix d'un gran estudi previ per la seva posterior aplicació. A costa de les seves grans avantatges que ofereix a nivell de dinàmica vehicular, el fet de mantenir el tren de potència a una temperatura de treball òptima és un repte abordat en aquest projecte, essent el principal objectiu definir un sistema de refrigeració líquida adient. Aquest es composa d'un intercanviador de calor per als inversors – els dispositius electrònics que més calor dissipen de tot el cotxe -, un altre per als propis motors, un radiador capaç d'evacuar tota aquesta energia i una bomba capaç de subministrar el caudal necessari d'aigua al sistema. A més a més, es proposa com a material principal per l'intercanviador de calor del motor el niló imprès en 3D, amb el propòsit de facilitar la fabricació del mateix i reduir dràsticament el seu pes. No obstant això, es conclou que el sistema dissenyat no és viable per aquesta aplicació, degut a les altes temperatures aconseguides al motor per culpa de la baixa conductivitat tèrmica d'aquest material.

Resumen

La incorporación de un sistema al tren de potencia de motor a rueda para un vehículo de Formula Student requiere de un gran estudio previo para su posterior aplicación. A expensas de las ventajas que ofrece a nivel de dinámica vehicular, el hecho de mantener todo el tren de potencia a una temperatura de trabajo óptima es un reto abordado en este proyecto, siendo el principal objetivo definir un sistema de refrigeración líquida adecuado. Éste se compone de un intercambiador de calor para los inversores - los dispositivos electrónicos que más calor disipan del vehículo -, otro para los propios motores, un radiador capaz de evacuar toda esta energía y una bomba capaz de suministrar el caudal necesario de agua al sistema. Para ello, se realizan estudios analíticos, estudios numéricos y estudios experimentales. Además, se propone como material principal para el intercambiador de calor del motor el nailon impreso en 3D, con el propósito de facilitar la fabricación del mismo y reducir drásticamente su peso. Sin embargo, se concluye que el sistema diseñado no es viable para susodicha aplicación, debido a las altas temperaturas alcanzadas en el motor por culpa de la baja conductividad térmica de dicho material.

Abstract

The incorporation of an in-wheel motor system to the powertrain of a Formula Student car requires an important previous study for its posterior application. Despite the great advantages that it offers at a dynamical level, the fact of keeping the whole powertrain system at an optimal temperature range is a challenge tackled in this project, being the principal objective to define an adequate liquid cooling system. This is composed by the inverter's heat exchanger – the electronic device which dissipates more heat inside the vehicle -, another heat exchanger for the motor – called cooling block -, a radiator capable of evacuating all this energy and a water pump capable of providing the needed mass flow rate to the system. In order to do that, it is carried out an analytical study, a numerical and an experimental one. Furthermore, it is proposed 3D printed nylon as the principal material for the motor cooling block, aiming to facilitate the manufacturing process and to dramatically reduce its weight. However, it is concluded that the designed system is unviable for that application due to the high temperatures reached in the motor due to the low thermal conductivity of the nylon.

Agradecimientos

Quisiera agradecer a diferentes personas e instituciones su existencia y/o colaboración, ya que gracias a ellos ha sido posible la realización de este trabajo.

Primeramente, dar las gracias a las instituciones académicas, concretamente a la Universitat Politècnica de Catalunya y a todos sus profesores, los cuales me han dado las herramientas necesarias para poder formarme como ingeniero y realizar este proyecto. Más especialmente a mi tutor, el doctor Alfredo Guardo Zabaleta, por todo su apoyo e implicación en todo momento a lo largo de todo este tiempo.

Por otro lado, quiero agradecer al equipo e-Tech Racing y a todos sus integrantes, tanto los que están como los que han estado, la motivación y la pasión con la que siempre han trabajado, siendo fuente de inspiración para la realización de este trabajo, así como una piedra angular tanto en mi carrera académica como profesional. Concretamente, mencionar a Bernat Torrents y a Javier Millet por su gran ayuda y compañerismo.

Por último, y no por ello menos importante, quiero dar las gracias a mis padres y a mi familia por ser mi principal punto de apoyo, tanto en los buenos como en los malos momentos, así como a mis amigos y compañeros de piso por su indiscutible apoyo incondicional.

Glossary

CAD	Computer Aided-Design
CAE	Computer Aided-Engineering
CFD	Computational Fluid Dynamics
y+	Wye plus
ABS	Acrylonitrile Butadiene Styrene
PLA	Polylactic Acid
HDT	Heat Deflection Temperature
VAT	Value Added Tax

Index

ANNEX B. RADIATOR MEASUREMENTS AND TEMPERATURE PLOTS. _____

List of figures

List of tables

1. Preface

The existence and motivation of the present work is only due to the Formula Student team e-Tech Racing and its competition, which generate the necessity of including their description in this section.

1.1. Formula Student

Formula Student is an international competition which challenges teams of universities from around the world to conceive, design, fabricate, develop and compete with small, formula style, race cars. Its main objective is to educate engineering students through the design and manufacture of these race cars, as well as bringing students closer to real world challenges.

This competition was born in the US in 1981 and coordinated by the Society of Automotive Engineering (SAE) under the name of Formula SAE. Later on, a partnership between the SAE and a European society made possible the expansion of the competition, being called Formula Student. Nowadays, the competition has evolved and it is split into three different classes: Internal Combustion Engine Vehicle (CV), Electric Vehicle (EV) and Driverless Vehicle (DV) (either CV or EV).

In order to carry out an evaluation of the work done by each team, numerous events take place during the competition, being clearly differentiated between static and dynamic events. Those events try to prove the reliability and competitiveness of the cars, as well as the vehicle design or the team's ability to develop a business model to sell and manufacture them with a rewarding profit. More specifically, the competition rewards with a maximum punctuation of 1000 points, which 675 correspond to dynamic event points, and the 325 remaining points, to the static ones.

It is interesting to know further about the competition events in order to better understand the challenge imposed by the competition itself. Therefore, we may enumerate all the static and dynamic events.

1.1.1. Static events

The static events approximately represent the 32% of the total punctuation, with a distribution of 325 points in the following manner:

- Business Plan Presentation Event (BPP) (75 points). The objective of the BPP is to evaluate the team's ability to develop and deliver a comprehensive business model which demonstrates the product (a prototype race car) could become a rewarding business opportunity. The judges of the event are treated like potential investors for the presented business model.

- Cost and Manufacturing Event (100 points). The objective of the cost and manufacturing event is to evaluate the team's understanding of the manufacturing processes and costs associated with the construction of a prototype race car. This includes trade off decisions between content and cost, make or buy decisions and understanding the differences between prototype and mass production.
- Engineering Design Event (150 points). The most valuable static event. The concept of the design event is to evaluate the student's engineering process and effort that went into the design of a vehicle.

Besides, every team has to meet the requirements specified by the competition regulation, which forces them to pass an arduous scrutineering process before entering any dynamic event.

1.1.2. Dynamic events

As we have previously stated, the dynamic events try to prove the dynamic behaviour and reliability of the car, being awarded 675 points as follows:

- Acceleration (75 points). The acceleration course is a straight line with a length of 75 m from starting line to finish line, where the course is at least 5 m. Time is measured from the starting line to the finish line.
- SkidPad (75 points). The skidpad course consists of two pairs of concentric circles in a figure of eight pattern. Two turns must be given in each direction (clockwise and counter clockwise), and the final measured time is the average of the best in each direction, as shown in Figure 1.1.

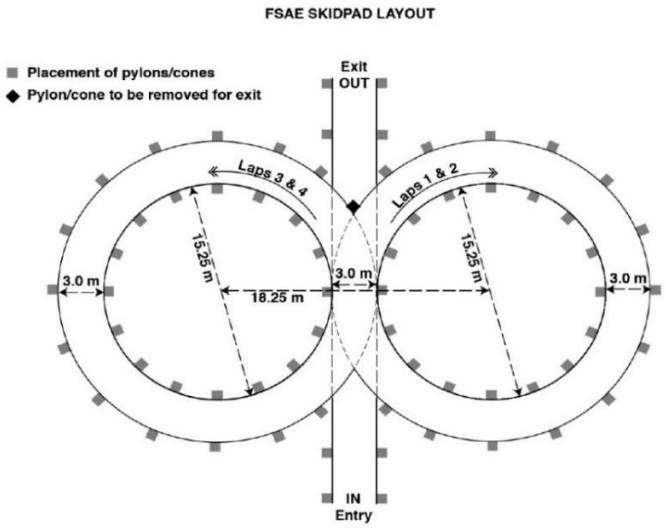

Figure 1.1 Skidpad event layout

- Autocross (100 points). The autocross track consists of a challenging one, with a length lesser than 1.5 km, containing straights, constant turns, slaloms, chicanes and other track requirements.
- Endurance (325 points). The most challenging dynamic event. Consists of the same track as in the autocross, but with an approximate length of 22 km, where the reliability of the car is showed.
- Efficiency (100 points). The efficiency event takes place at the same time the endurance does it, measuring the energy consumption in the event and the time it has taken to the team to complete the event.

1.2. e-Tech Racing

EEBE e-Tech Racing is a Formula Student team which belongs to the Escola d'Enginyeria de Barcelona Est (EEBE), from the Universitat Politècnica de Catalunya (UPC) and competes in the competition with an electric vehicle (EV).

Figure 1.2 e-Tech Racing car during the Formula Student Czech Republic 2017 competition

This team, which is composed by forty engineering students from different industrial branches (mechanical, electric and electronic engineering students), is the reason of the present work, the design of a cooling system of an electric Formula Student car. The 2016/2017 season's car is represented in Figure 1.2.

E-Tech Racing was created in 2013 in Escola Universitaria d'Enginyeria Tècnica Industrial de Barcelona (EUETIB), from UPC, participating in Formula Student in the electric vehicle class. Every year the team has managed to design and build a completely new car, directly involving the design of a cooling system

that enables the car to compete at the highest power requirements without struggling in reliability. This has become a challenge every season, since the power availability and management knowledge has increased, demanding a more efficient cooling system year after year.

A remarkable change took place in 2016/2017 season, when a Catalan company called Vernis Motors decided to support the team by providing it with custom-made motors, one for each rear wheel. Moreover, in order to take maximum profit out of them, new electronic inverters were acquired, bringing the cooling system department a new defiance. Due to time-constraints and lack of knowledge, the custom-made motors were cooled down by air-forced convection, seen in Figure 1.3, while the inverters used liquid cooling.

Figure 1.3 Custom-made motor provided by the motor case to cool it down during 2016-2018 seasons.

Therefore, the cooling system consisted of the air-motor cooling, the inverter's liquid cooling and the air-cooled battery package. However, during the competition high temperatures were reached in the electric motors due to a lack of air flow through the finned motor-case, and the motors' controllers suffered from them too due to the absence of air bleeding through the liquid cooling circuit.

By the time this work is written, a new cooling system has been designed for the 2017/2018 season, maintaining the same cooling motor case and motor controllers but with a different battery package distribution and improved air flow through all the thermal devices. In Figure 1.4 can be observed the motor cooling concept for 2017/2018 season.

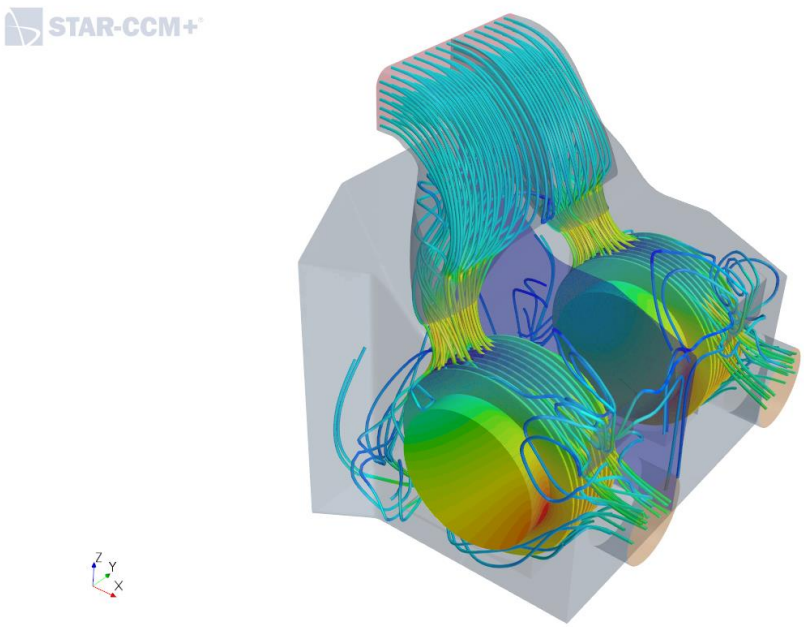

Figure 1.4 Motor cooling design concept for the 2017/2018 season.

1.3. Motivation

Becoming part of e-Tech Racing as a member of the cooling system's department allowed me to investigate further in heat exchangers and heat transfer methods from an analytical and computational point of view. Therefore, after completing two years in the team, it permitted me to take heat transfer and fluid dynamics as some of the pillars of my professional career, and selecting this topic was the perfect opportunity to dive even deeper in this engineering field. Furthermore, this is the first time an in-wheel motor cooling system is designed for e-Tech Racing ever, arousing even more my motivation around this project.

1.4. Previous requirements

The previous requirements to carry out this project involved theoretical and numerical knowledge about fluid mechanics and heat transfer analysis. The theoretical knowledge was provided by the university with subjects like Thermal Engineering and Fluid Mechanics which consolidate the basic equations entailing these phenomena, as well as numerical approaches. For both subjects, heat exchangers selection and heat transfer and pump selection and hydraulic circuit calculations, respectively, were basic aspects that allowed the creation of this project. Besides, some basic manufacturing knowledge was necessary in this work, like drilling, machining or 3D printing concepts.

On the other hand, taking part of the e-Tech Racing Formula Student team allowed us to work with professional numerical simulation software which brings the opportunity to work out numerical calculations with an impressive speed and accuracy. Nevertheless, it is indispensable to know how to use these tools and becoming part of this team permitted such learning process.

2. Introduction

As it was mentioned in the previous chapter, the purpose of this work is to present the design of a cooling system of an electric Formula Student car for the team EEBE e-Tech Racing. More specifically, an in-wheel motor cooling system for a potential new car for the upcoming seasons.

2.1. Objectives

The objective of this project is to present an in-wheel motor cooling system for the e-Tech Racing Formula Student team that allows maximum overall car performance without leading to temperature problems.

2.1.1. Specific objectives

Being stated the objective of this work, some specific objectives may be described in order to achieve the general one. All of them are described as follows:

- Design a Cold Plate to cool down the motor controllers and a motor cooling block.
- Do not reach 135ºC in any motor.
- Minimise weight and pressure drop within all cooling system devices.
- Choose a heat exchanger through real testing.
- Choose a water pump for the cooling system.
- Check all the formal aspects of this project, including the bibliography.

Consequently, the whole system will be based on these requirements.

2.2. Project scope

In order to reach these specific objectives, the project scope is listed in the following points:

- Design the geometry of the water channels inside the cooling devices (motor controllers and motors) through CAD modelling, as well as the geometry of the devices themselves.
- Introduce basic theoretical knowledge about heat transfer, fluid mechanics and CFD.
- Work out simple analytical calculations to get an approximation of the ideal cooling system.
- Carry out a CFD study for each cooling device, which includes grid independence studies.
- Test a radiator, more specifically the STD116, a heat exchanger manufactured by Setrab, in order to prove its performance.

Therefore, this project presents the motor controllers cooling as well as the in-wheel motors cooling design and the whole system selection. Nevertheless, it does not contain information about the cooling system assembly inside the vehicle, since other departments are involved in this task.

3. Powertrain cooling requirements

In order to design the in-wheel motor cooling system, it was proposed a liquid cooling circuit that could cool down the following powertrain devices:

- Four motor controllers (one for each motor).
- Four in-wheel motors.
- Two radiators located outside the car in order to cool down the circuit.
- Two water pumps.

Water circulated through all of these devices, and the whole system was decomposed into two independent cooling circuits as it is shown in Figure 3.1.

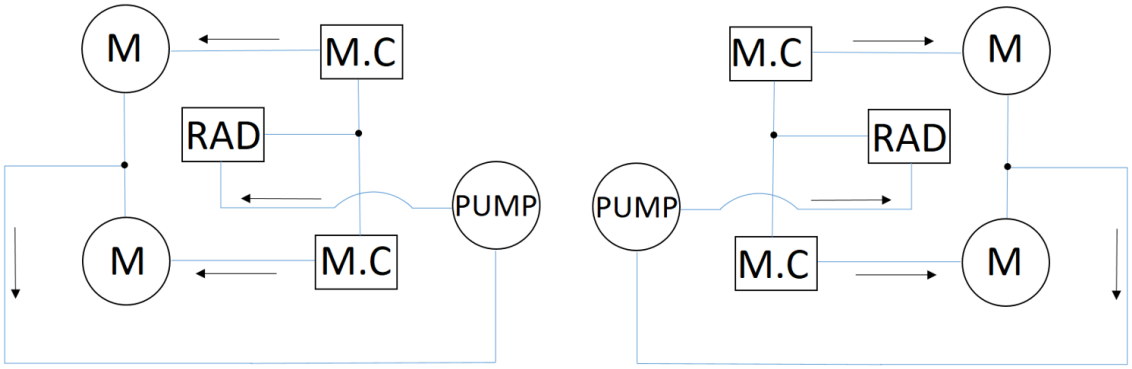

Figure 3.1 Schematic of the cooling system for the in-wheel motor powertrain system.

This schematic shows the position of each device in the circuit, where M.C stands for Motor Controller, M for Motor, RAD for Radiator and PUMP for water pump. Each motor is coupled to each wheel, the radiators are kept outside the vehicle to let the air flow through them and every motor controller is connected to its correspondent motor. The connection order was imposed by the temperature range of each device, which is explained in section 5.

3.1. Inverter's cooling

The motor controllers (also called inverters) are the electronic devices that transform the DC current emerging from the batteries into AC current to the motors. More specifically, inside this device we find what are called the IGBT's (Insulated-Gate Bipolar Transistor), a semiconductor device which is used as an electronic switch. Therefore, the IGBT's are the main responsible of this transformation and, in fact, the devices which more energy consume inside the inverters.

Hence, appears the necessity of controlling its working temperature, since this is a critical device inside the car and, if a maximum temperature is surpassed, due to safety reasons, it turns off, also completely turning off the vehicle. So, the working priority of this device is maximum, and a cooling system for it must be coupled.

A liquid cooling has to be used and the thermal device responsible to do so is called Cold Plate or heat sink. This is a heat exchanger that has been used in all the e-Tech Racing cars. In Figure 3.2 can be appreciated the motor controller of seasons 2016/2017 and 2017/2018, as well as the Cold Plate used, respectively.

Figure 3.2 Motor controller used in 2016/2017 and 2017/2018 seasons and its Cold Plate, mounted under the inverter.

Water flows through the Cold Plate through a machined water channel, which absorbs the heat delivered by the IGBT's located just above the Cold Plate. In this case, the heat exchanger was provided by the manufacturer, who recommended a volumetric flow rate of 12 LPM through it in order to keep the IGBT's at an indicated safe temperature range.

As it may be thought, the objective of this device is to provide a good temperature range while performing the minimum pressure loss across the circuit.

3.1.1. Inverter's specifications

So, in order to be able to start the design process, the inverter's specifications were delivered by the Motors & Inverters department, which proposed the following motor controller for the in-wheel motor design: Gold Drum HV (High Voltage) Digital Servo Drive, by Elmo Motion Control Ltd., shown in Figure 3.4.

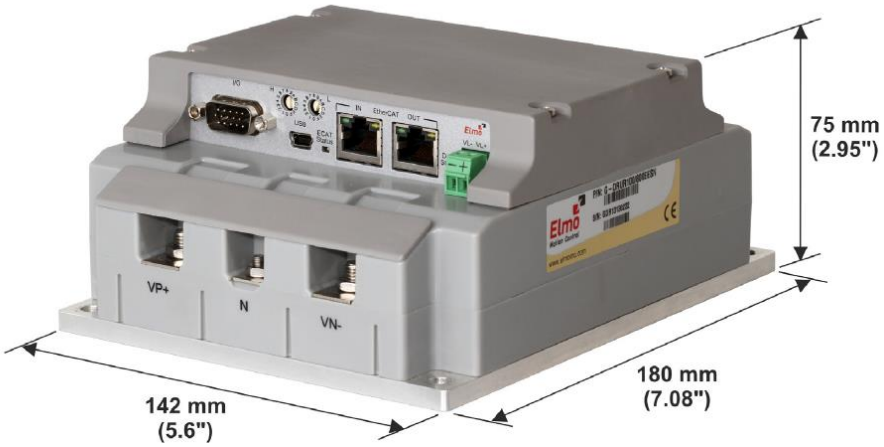

Figure 3.3 Elmo's Gold Drum HV motor controller (Source: Elmo Motion Control Ltd.).

The technical data provided by the manufacturer is presented in Table 3.1.

Feature	Units	35/800	50/800	R70/800	R100/800
Minimum supply voltage	VDC	*For H, S, T, or A option = 95			
Nominal supply voltage	VDC	560 for 400 VAC 680 for 480 VAC			
Maximum supply voltage	VDC	780			
Maximum continuous power output	kW	22.5	32.5	45	65
Efficiency at rated power (at nominal conditions)	%	> 98			
Auxiliary supply voltage option	VDC	18 to 30 VDC (only in H, S, T, or A option)			
Auxiliary power supply	VA	≤5 VA without external loading ≤7 VA with full external loading			
Continuous current limit (Ic) Amplitude sinusoidal/DC trapezoidal commutation	A	35	50	70	100
Continuous RMS sinusoidal commutation current limit (Ic)	A	25	35	50	71
Peak Current	A	70	100	No Peak	No Peak

Table 3.1 Technical data of the 800V Gold Drum HV motor controller (Source: Elmo Motion Control Ltd.).

The model selected allowed a maximum of 800V with a continuous current limit of 100A (the last column, R100/800), providing a maximum power of 65kW. This model was selected since the maximum power it delivered did not exceed the maximum power imposed by the competition, which is 80kW.

In addition, thermal data was also provided as follows:

- Shut-off temperature: 86 to 88ºC.
- Thermal resistance when connecting to an N5 roughness metallic surface external heat sink: 0.07 ºC/W. If a thermal compound is used: 0.03ºC/W.

Furthermore, a power dissipation chart was available, which referred to the power dissipated depending on the RMS current. In our case, it was calculated a use of 518Vdc, which is similar to the 560Vdc red curve plotted in Figure 3.6. Therefore, looking at the graph, at a maximum current RMS of 71A, the resulting power dissipated was, approximately, 300W.

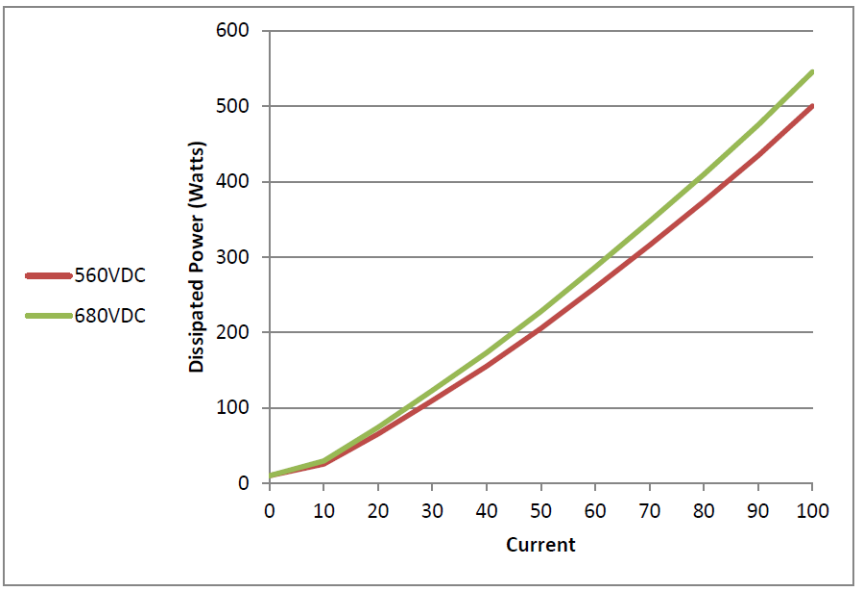

Figure 3.4 Power dissipation of the Gold Drum HV motor controller (Source: Elmo Motion Control Ltd.).

So, with the power dissipation data at maximum RMS current and maximum temperature allowed by the device, the design of a Cold Plate for the new motor controller could be started.

3.2. In-wheel motor cooling

The new incorporation to the vehicle powertrain was the arrival of in-wheel motors. In this case, the same company that had built the costume motors for the previous seasons (Figure 1.3) decided to manufacture these in-wheel motors for the e-Tech Racing team. It was a Permanent Magnet

Synchronous Motor (PMSM), which consisted of a rotor with a number of permanent magnets (in this case 8 poles) and a stator with phase windings that provides a rotating field which the PM rotor follows (Hooper, 2011). In order to cool it down, a liquid cooling heat exchanger, called motor cooling block, had to be incorporated.

We may find an example in Figure 3.5. Other Formula Student teams have been incorporating this powertrain for years, proving its great performance compared to other powertrain systems.

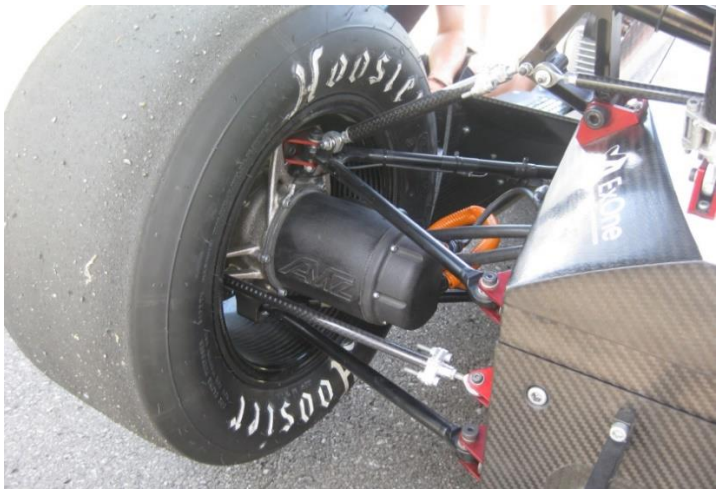

Figure 3.5. In-wheel motor of the 2013 AMZ Formula Student team car (Source: Styger, 2014).

3.2.1. In-wheel motor specifications

Motor losses	Losses (W)	Losses (%)
Stator winding losses	266.44	22.01
Iron losses	821.74	67.87
Mechanical losses	45.92	3.79
Rotor losses	9.93	0.82
Additional losses	66.67	5.51
TOTAL LOSSES	**1210.70**	**100.00**

Table 3.2 Power dissipation of the in-wheel motor developed by Vernis Motors (Source: Vernis Motors SL.).

As so, the stator and the rotor geometry have been developed by this company, as well as all the power dissipation inside the motor. The motor losses may be appreciated in Table 3.2.

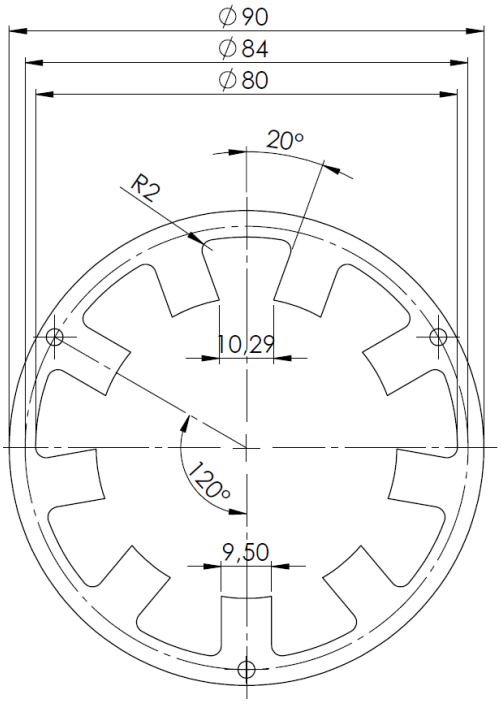

Figure 3.6 Stator and rotor geometry of the in-wheel motor (Source: Vernis Motors SL.).

Besides, other geometrical parameters were delivered by the manufacturer, as it might be seen in Figure 3.6:

- Yoke width: 5mm
- Stacked plate length: 70mm
- Head winding (cables exit): 20mm
- Head winding (other side): 15mm

Those basic parameters allowed the possibility of drawing a 3D CAD representation in order to start the cooling block design.

3.3. Design requirements and limitations

Therefore, the design requirements for this system were to dissipate the 300W of the motor controllers for each circuit, as well as the 1210.70W of the in-wheel motors. More specifically, to not exceed 86ºC and 135ºC, respectively. Besides, the fluid velocity inside the heat exchangers could not surpass a value of 3 m/s nor be under 1 m/s in order to avoid fouling inconveniences or depositions inside them, respectively. On the other hand, weight is always an important factor in vehicle dynamics, granting better results with lighter devices. As a consequence, it was important to reduce the weight of the heat exchangers and the pressure drop across them, so less energy would be needed to pump the fluid, leading to smaller batteries and smaller pumps.

However, due to competition rules, some limitations were applied into this project. Thus, the competition rules that directly affect this design were the following:

- *''T6.2.1: Water-cooled engines must only use plain water. Electric motors, accumulators or HV electronics may only use plain water or oil as the coolant.''*
- *''T6.3.1: Any cooling or lubrication system must be sealed to prevent leakage.''*
- *''EV2.1.2: The rotating part of the motor must be contained within a structural casing where the thickness is at least 3.0 mm (0.120 inch) for Aluminium alloy 6061-T6 or 2.0 mm (0.080 inch) for steel. The motor casing may be the original motor casing, a team built motor casing or the original casing with additional material added to achieve the minimum required thickness. If lower grade Aluminium Alloy is used, then the material must be thicker to provide an equivalent strength.''*

Consequently, the fluid to be used was water and the electric motor needed to be contained within an aluminium alloy 6061-T6 – or better – 3mm thick.

So, the whole system design was based on these requirements.

4. Theoretical framework

As it was mentioned in the previous requirements chapter, some theoretical knowledge had to be used in this project in order to carry out the cooling system's design. Since theoretical concepts acquired during the bachelor like heat transfer and fluid mechanics until numerical methods to apply those theoretical concepts.

4.1. Heat transfer and fluid mechanics

In order to begin the design process, some fundamental concepts had to be clarified. Those concepts refer to: heat transfer, that explains the thermal behaviour of the cooling system and fluid mechanics, so we know the water pressure drop across the devices, as well as initial fluid flow behaviour consideration. Consequently, we now describe the equations that rule these phenomena.

4.1.1. Heat transfer

Heat may be defined as a way of transferring energy from one mass to another by a temperature difference between both bodies. This temperature difference is achieved, in this case, by the circulation of cold plane water over hot surfaces and this water flow rate is decided upon the heat we need to remove from our electronic devices.

We need to define the heat transfer methods to dissipate such generated heat, which are conduction and convection. It has to be noted that radiation effects were not taken into account in this design, since the radiation heat transfer phenomena were insignificant compared to conduction and convection effects.

4.1.1.1. Conduction

''Conduction is the transfer of energy from the more energetic particles of a substance to the adjacent less energetic ones as a result of interactions between the particles'' (Cengel YA 2006). It is defined by the Fourier's law of heat conduction.

$$\dot{Q} = -kA\frac{\partial T}{\partial x} \qquad \textbf{(Eq. 4.1)}$$

where k is the thermal conductivity of the material, *A* the heat transfer area and $\frac{\partial T}{\partial x}$ the temperature gradient in a direction x.

Besides, this equation can be written in terms of the thermal resistance of the material as

$$\dot{Q} = \frac{\Delta T}{R} = \frac{\Delta T}{\frac{kA}{L}} \quad \textbf{(Eq. 4.2)}$$

where R is the thermal resistance of the material in a given direction of a given thickness L, thermal conductivity k and heat transfer area A.

4.1.1.2. Convection

Convection is the heat transfer phenomenon which occurs between a fluid in motion and a solid surface. There exists natural and forced convection, but in this project we have only taken into account the forced convection where the fluid is forced to flow over the surface. It is defined the Newton's law of cooling as

$$\dot{Q} = hA_s(T_s - T_\infty) \quad \textbf{(Eq. 4.3)}$$

where h is the convection heat transfer coefficient, A_s is the surface area through which convection takes place, T_s is the surface temperature and T_∞ is the fluid temperature sufficiently far away from the surface.

Besides, the previous equation can be written as follows, assuming steady-state internal flow inside a tube

$$\dot{Q} = hA_s\Delta T_{ln} \quad \textbf{(Eq. 4.4)}$$

where ΔT_{ln} is the logarithmic temperature difference:

$$\Delta T_{ln} = \frac{T_i - T_e}{ln(\frac{T_s - T_e}{T_s - T_i})} \quad \textbf{(Eq. 4.5)}$$

taking T_i the inlet temperature and T_e the exit temperature.

Furthermore, energy conservation had been taken into account, providing the following equation

$$\dot{Q} = \dot{m}C_p\Delta T \quad \textbf{(Eq. 4.6)}$$

where $\dot{m}$ is the mass flow rate, C_p the isobaric specific heat and ΔT is the temperature difference between the exit and the inlet of the control volume. Potential and kinetic energy variations had been ignored.

Finally, the Nusselt number was defined as

$$Nu = \frac{hD_H}{k} \quad \textbf{(Eq. 4.7)}$$

where *k* is the thermal conductivity of the fluid. On the other hand, the Nusselt number could be written in terms of the friction factor *f* and the Reynolds and Prandtl number as the Gnielinski equation:

$$Nu = \frac{\left(\frac{f}{8}\right)(Re - 1000)Pr}{1 + 12.7\left(\frac{f}{8}\right)^{0.5}(Pr^{\frac{2}{3}} - 1)} \quad \textbf{(Eq. 4.8)}$$

where the Prandtl number is defined as $Pr = \frac{\mu C_p}{k}$, Re is the Reynolds number and f the friction factor.

4.1.2. Fluid mechanics

The cooling system used plane water as a coolant, as it was imposed by the competition rules. This fluid was contained in a closed circuit, so the main factor we were looking for was the total pressure drop across the system in order to select a pump to satisfy our needs. Besides, some non-dimensional number like the Reynolds number would describe the flow regime, a quantity of interest for the design.

4.1.2.1. Reynolds number

The Reynolds number is a non-dimensional number which is the ratio of inertial over viscous forces on a fluid. It is expressed as

$$Re = \frac{\rho c D_H}{\mu} \quad \textbf{(Eq. 4.9)}$$

where ρ is the fluid density, c is the fluid velocity, D_H is the characteristic diameter of the fluid and μ the dynamic viscosity of the fluid.

On the other hand, the hydraulic diameter is defined as

$$D_H = \frac{4A}{p} \quad \textbf{(Eq. 4.10)}$$

where A is the cross-section the fluid goes through, and p is the perimeter of that cross-section.

4.1.2.2. Pressure drop

Pressure drop across the system is defined by the following expression:

$$\Delta P = \sum_{i=1}^{n} k_i \cdot \dot{V}_w^2 \quad \textbf{(Eq. 4.11)}$$

where ΔP is the total pressure drop across the system, k_i is the pressure drop coefficient across each device and $\dot{V}_w$ is the water volumetric flow rate across the system. The pressure drop coefficient is defined as

$$k_i = \frac{\Delta P_i}{\dot{V}_i^2} \quad \textbf{(Eq. 4.12)}$$

where ΔP_i is the pressure drop across a hydraulic element (pump, radiator, motor controller, Cold Plate, motor, tube and other accessories) and $\dot{V}_i$ is the volumetric flow rate through that element.

The pressure drop across a tube is written as

$$\Delta P_{tube} = \rho \frac{c^2}{2} f \frac{L}{D_H} \quad \textbf{(Eq. 4.13)}$$

where f is the friction factor and L is the tube's length.

So, we need to define the friction factor. For a turbulent regime, according to the Darcy's Law, the friction factor is expressed as

$$f = \frac{1.325}{(ln\left(\frac{\varepsilon}{3.7D_H}\right) + \frac{5.74}{Re^{0.9}}))^2} \quad \textbf{(Eq. 4.14)}$$

where ϵ is the surface's roughness where the fluid flows through.

4.2. CFD fundamentals

With the previously mentioned equations there are some considerations that were not taken into account. For example, pressure losses along the circuits due to boundary layer separation, heat transfer due to conduction and convection in non-regular areas that were extremely difficult to be analysed by analytical equations, such as the mentioned above.

This is why this work presents numerical calculations, which were used to obtain approximated solutions for velocity, pressure and temperature fields along the studied domain. The numerical calculations which allowed us to obtain this information were carried out through a computer, that conducted us to a scientific branch called Computational Fluid Dynamics (CFD). It is the science of predicting fluid flow, heat transfer, mass transfer, chemical reactions and related phenomena by solving the mathematical equations which govern these processes using numerical methods (Bakker 2006). Its main application is to provide complementary data to the theoretical calculations.

Basically, CFD consists on mathematically modelling the physical problem we want to solve involving the aforementioned phenomena, where the governing equations (continuity, momentum and energy equations) are solved in order to obtain the properties of the fluid being studied by applying numerical methods. In this case, a commercial software was used to work out the numerical methods, called STAR-CCM+, a Computational Aided Engineering (CAE) software provided by SIEMENS. Therefore, the mathematical foundation of the numerical methods used in CFD are presented - more specifically the STAR-CCM+ methodology - as well as basic discretization methods and turbulence modelling.

The following definitions and equations were mainly extracted from the Theory Guide of the STAR-CCM+ documentation.

4.2.1. Fundamental equations

On a macroscopic scale, where the typical lengths are much greater than the inter-atomic distances, the discrete structure of matter can be neglected and materials can be modelled as continua. The mathematical models that describe the physics of continua are derived from fundamental laws that express conservation principles. In this case, the conservation laws for a continuum are expressed using a Eulerian approach, where a given volume represents a portion of space where material can flow through.

Thus, the fundamental laws that govern fluid mechanics are the conservation of mass, linear momentum and energy (presented here in differential form for an infinitesimal control volume).

4.2.1.1. Conservation of mass

The balance of mass through a control volume is expressed by the continuity equation:

$$\frac{\partial \rho}{\partial t} + \nabla \cdot \left(\rho \underline{v}\right) = 0 \qquad \textbf{(Eq. 4.15)}$$

Where ρ is the density and $\underline{v}$ the continuum velocity.

4.2.1.2. Conservation of linear momentum

The time rate of change of linear momentum is equal to the resultant force acting on the continuum:

$$\frac{\partial(\rho\underline{v})}{\partial t} + \nabla \cdot (\rho\underline{v} \otimes \underline{v}) = \nabla \cdot \underline{\underline{\sigma}} + \underline{f_b} \qquad \textbf{(Eq. 4.16)}$$

where $\otimes$ is the tensorial (Kronecker) product, $\underline{f_b}$ is the resultant of the body forces (such as gravity and centrifugal forces) per unit volume acting on the continuum, and $\underline{\underline{\sigma}}$ is the stress tensor. For a fluid, the stress tensor is often written as sum of normal stresses and shear stresses as follows:

$$\underline{\underline{\sigma}} = -p\underline{\underline{I}} + \underline{\underline{T}} \qquad \textbf{(Eq. 4.17)}$$

where $\underline{\underline{I}}$ is the identity matrix, p is the pressure and $\underline{\underline{T}}$ the viscous stress tensor, giving the following expression for the linear momentum equation:

$$\frac{\partial(\rho\underline{v})}{\partial t} + \nabla \cdot (\rho\underline{v} \otimes \underline{v}) = -\nabla \cdot \left(p\underline{\underline{I}}\right) + \nabla \cdot \underline{\underline{T}} + \underline{f_b} \qquad \textbf{(Eq. 4.18)}$$

4.2.1.3. Conservation of energy

When the first law of thermodynamics is applied to the control volume, the conservation of energy can be written as

$$\frac{\partial(\rho E)}{\partial t} + \nabla \cdot (\rho E\underline{v}) = \underline{f_b} \cdot \underline{v} + \nabla \cdot \left(\underline{v} \cdot \underline{\underline{\sigma}}\right) - \nabla \cdot \underline{q} + S_E \qquad \textbf{(Eq. 4.19)}$$

Where E is the total energy per unit mass, $\underline{q}$ is the heat flux and S_E is an energy source per unit volume.

In most cases, the partial differential equations of a mathematical model are not a closed set, that is, the number of unknown quantities exceeds the number of equations. To provide closure, additional equations are added to the mathematical model (also called constitutive laws). However, due to the project scope of this work, we will not dive into detailed equations. Simple concepts are provided in order to understand the CFD methodology.

4.2.2. Discretization methodology and fluid flow equations

Once we have defined the fluid governing equations, a discretization method is carried out to convert the continuous system of equations to a set of discrete algebraic equations, which can be solved using numerical techniques, as it is shown in the example of Figure 4.1.

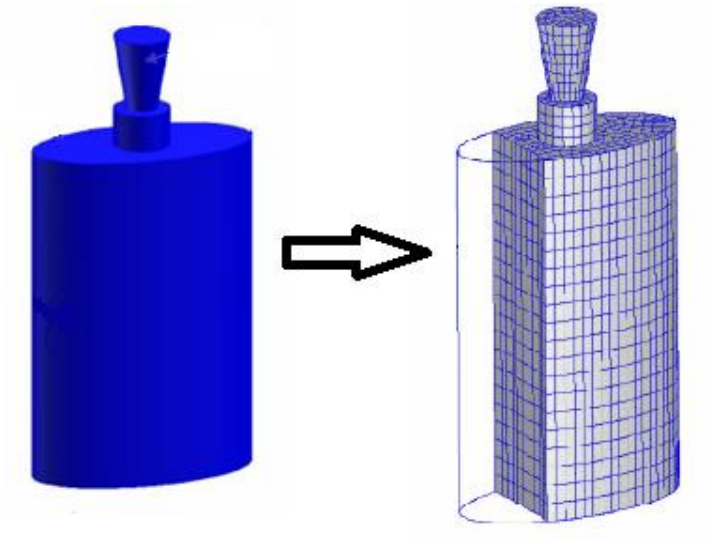

Figure 4.1 Example of a water bottle and its discretized domain, respectively (Bakker 2006)

The discretization method emulates the following procedure:

- The continuous domain is divided into a finite number of subdomains, also called grid or mesh.
- The unknowns are stored at specific locations of the mesh (vertices, cell centroids, face centroids or edges).
- An integral or weak form of the differential equations is employed for spatial discretization.

For the case we are working with, STAR-CCM+ discretizes the continuous equations using the Finite Volume Method (FVM). Fundamentally, by using the FVM we are handling with the Reynolds Transport theorem applied to each control volume of the subdivided domain (mesh cell).

For further information, the reader is suggested to explore the *STAR-CCM+ Documentation*.

4.2.3. Turbulence modelling

When analysing fluid flow, it is well-known the appearance of irregular fluctuating flow quantities, also called turbulences. These fluctuations may appear at such small scales and high frequencies that resolving them in time and space comes at excessive computational costs. Consequently, instead of solving the exact governing equations of turbulent flows, it is less expensive to solve for averaged quantities and approximate the impact of the small fluctuating structures.

In this work, the Reynolds-Averaged Navier-Stokes (RANS) turbulence model was used, more specifically an Eddy viscosity model called Shear-Stress Transport (SST) K-Omega.

4.2.3.1. Reynolds-Averaged Navier-Stokes turbulence model

RANS turbulence models provide closure relations for the RANS equations, that govern the transport of the mean flow quantities. To obtain the Reynolds-Averaged Navier-Stokes equations, each solution variable ϕ in the instantaneous Navier-Stokes equations is decomposed into its mean (or averaged) value $\bar{\phi}$ and its fluctuating component ϕ':

$$\phi = \bar{\phi} + \phi' \qquad \textbf{(Eq. 4.20)}$$

where ϕ represents velocity components, pressure, energy or species concentration. Inserting the decomposed solution variables into the Navier-Stokes equations results in equations for the mean quantities.

The mean mass and momentum transport equations can be written as:

$$\frac{\partial \rho}{\partial t} + \nabla \cdot \left(\rho \underline{\bar{v}}\right) = 0 \qquad \textbf{(Eq. 4.21)}$$

$$\frac{\partial \left(\rho \underline{\bar{v}}\right)}{\partial t} + \nabla \cdot \left(\rho \underline{\bar{v}} \otimes \underline{\bar{v}}\right) = -\nabla \cdot \left(\bar{p} \underline{\underline{I}}\right) + \nabla \cdot \left(\underline{\underline{T}} + \underline{\underline{T_t}}\right) + \underline{f_b} \qquad \textbf{(Eq. 4.22)}$$

where $\underline{\bar{v}}$ and $\bar{p}$ are the mean velocity and pressure, respectively.

These equations remain essentially identical to the original Navier-Stokes equations (Eq. 4.15 and Eq. 4.19), except that an additional term now appears in the momentum transport equation. This additional term is a tensor quantity $\underline{\underline{T_t}}$, known as the Reynolds stress tensor, which has the following definition:

$$\underline{\underline{T_t}} = -\rho \begin{pmatrix} \overline{u'u'} & \overline{u'v'} & \overline{u'w'} \\ \overline{v'u'} & \overline{v'v'} & \overline{v'w'} \\ \overline{w'u'} & \overline{w'v'} & \overline{w'w'} \end{pmatrix} \qquad \textbf{(Eq. 4.23)}$$

where u', v' and w' are the fluctuating fluid velocity components. The challenge is to model $\underline{\underline{T_t}}$ in terms of the mean flow quantities, and hence provide closure of the governing equations.

4.2.3.2. Eddy Viscosity model

One way of modelling the Reynolds stress tensor is through the Eddy viscosity models. Here appears the concept of a turbulent eddy viscosity μ_t, which makes possible the representation of the $\underline{\underline{T_t}}$ as a function of mean flow quantities. The most common model is known as the Boussinesq approximation:

$$\underline{\underline{T_t}} = 2\mu_t \underline{\underline{S}} - \frac{2}{3}(\mu_t \nabla \cdot \vec{v})\underline{\underline{I}} \qquad \textbf{(Eq. 4.24)}$$

where $\underline{\underline{S}}$ is the mean strain rate tensor.

It can be seen the assumption of considering a linear proportionality between the Reynolds stress tensor and the mean strain rate, which forces to not take into account anisotropic turbulence. The eddy viscosity models solve additional transport equations for scalar quantities that enable the turbulent μ_t to be derived. The one which has been chosen is the SST K-Omega model.

4.2.3.3. K-Omega turbulence model

The K-Omega turbulence model is a two-equation model that solves transport equations for the turbulent kinetic energy k and the specific dissipation rate ω (the dissipation rate ε per unit turbulent kinetic energy k) in order to determine the turbulent eddy viscosity (Wilcox 1988).

This model has been chosen over the K-Epsilon turbulence model (another eddy viscosity model) for several reasons. K-Omega model has an improved performance for boundary layers under adverse pressure gradients. Besides, it may be applied throughout the boundary layer including the viscous-dominated region. However, the main constraint of the original form of the K-Omega model is that boundary layer computations are sensitive to the values of omega in the free stream, which translates into extreme sensitivity to inlet boundary conditions for internal flows. Hence, a variant of the K-Omega model appears, called Shear-Stress Transport (SST) K-Omega (Menter 1994), that adds an additional non-conservative cross-diffusion term which, eventually, blends a K-Epsilon model in the far field with a K-Omega model near the wall, bringing together the benefits of these two models and avoiding the sensitivity problems previously mentioned.

Therefore, the turbulent eddy viscosity μ_t is calculated as:

$$\mu_t = \rho k T \qquad \textbf{(Eq. 4.25)}$$

where T is the turbulent time scale, which is dependent on the specific dissipation rate ω.

So, we need to compute the kinetic energy and the specific dissipation rate. We do it by adding two-transport equations, which are:

$$\frac{\partial}{\partial t}(\rho k) + \nabla \cdot \left(\rho k \underline{\bar{v}}\right) = \nabla \cdot [(\mu + \sigma_k \mu_t)\nabla k] + P_k - \rho \beta^* f_{\beta^*}(\omega k - \omega_0 k_0) + S_k \qquad \textbf{(Eq. 4.26)}$$

$$\frac{\partial}{\partial t}(\rho \omega) + \nabla \cdot \left(\rho \omega \underline{\bar{v}}\right) = \nabla \cdot [(\mu + \sigma_\omega \mu_t)\nabla \omega] + P_\omega - \rho \beta f_\beta(\omega k - {\omega_0}^2) + S_\omega \qquad \textbf{(Eq. 4.27)}$$

where: μ is the dynamic viscosity; σ_ω and σ_k are Model Coefficients; $P_{\boldsymbol{k}}$ and $P_{\boldsymbol{\omega}}$ are Production Terms; f_{β^*} is the free-shear modification factor; f_β is the vortex-stretching modification factor; S_k and S_ω are source terms; k_0 and ω_0 are ambient turbulence values and β is the thermal expansion coefficient. All these terms have a meaning, but due to the project scope, we will not investigate them.

5. Cooling system's design

The cooling system, as it was mentioned in section 3, consists of several devices: four motor controllers, four motors, two radiators and two water pumps. As both cooling systems were equal, we only studied one of them. Therefore, the cooling system studied was composed by two motors controllers, two motors, one radiator and one pump. In Figure 5.1 and Figure 5.2 are the CAD representations of the motor controllers and electric motors, according to the previous chapters' descriptions.

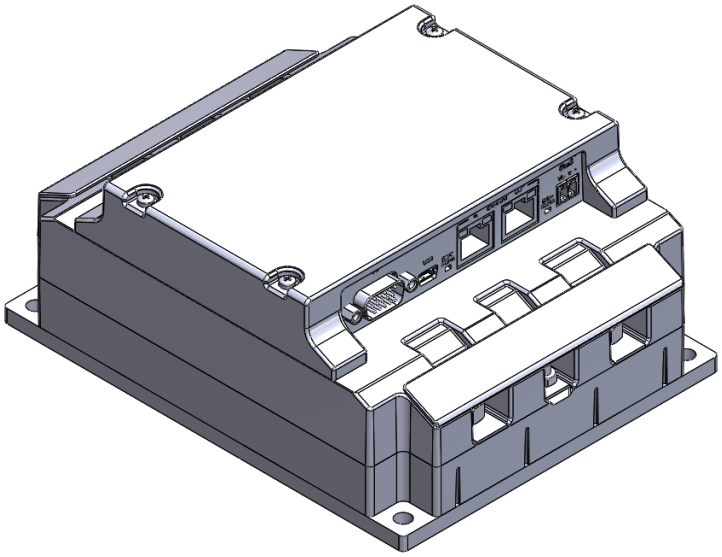

Figure 5.1 Elmo's motor controller CAD representation.

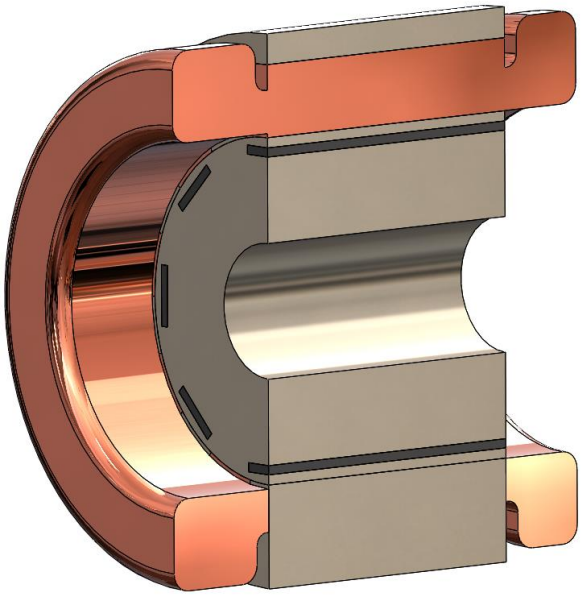

Figure 5.2 In-wheel motor CAD cross-section representation.

The motor controllers as well as the motors were connected in series. It is, the water flowed from the radiator to one motor controller and then to its correspondent motor. This was due to the thermal sensitivity of the devices, where the inverter was the most sensitive one due to its maximum allowable temperature. As it was said, the inverter's shut-off temperature was 86ºC, while the greatest temperature allowed at the motor was 135ºC. Then, it made sense to put the motor controller before the motor, since it would contain the coolest water of the circuit.

Consequently, the design of the cooling devices was dependent on one another. We could not finish the design of one device before finishing the other, so both designs had to be carried out at the same time.

5.1. Cold Plate design concept

Cold Plate final design was decided between two different concepts: a drilled Cold Plate and a machined Cold Plate. Both of them looked for the same objective but with different manufacturing costs.

Made out of aluminium, the Cold Plate design contemplated the water channel configuration as well as the material thickness. An example of Cold Plate design is represented in Figure 5.3, which was used as an initial design iteration.

Figure 5.3 Cold Plate configuration for the 2016-2018 motor controller (Source: BAMOCAR PG-D3 Manual V02)

5.2. Motor cooling block design concept

It is important to bear in mind the influences of other previous water-cooled electric motors in this design. There was another project related to this topic which could be called the base design in order to carry out a motor cooling block, conducted by an ex-member of the e-Tech Racing team. In that project, it was arrived to the conclusion that a helix water channel around the motor was the best possibility in terms of pressure drop and maximum temperatures (Torrents, 2018). As so, the present motor cooling block concept was pretended to be an evolution of this design, which is shown in Figure 5.4.

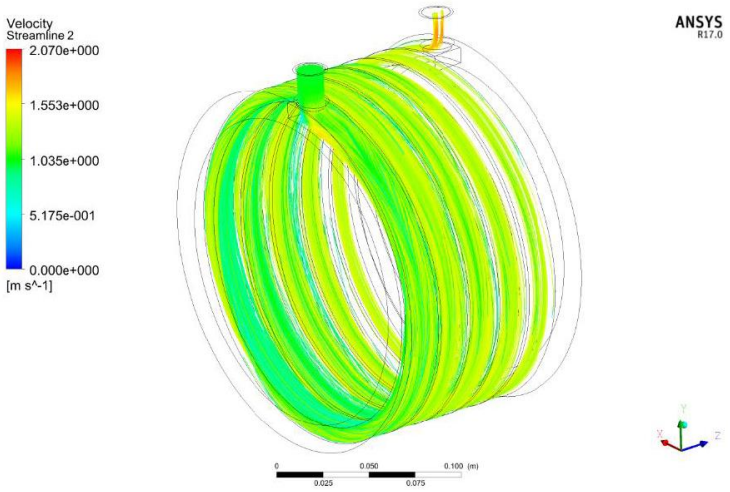

Figure 5.4 Water channel concept from previous works related to motor cooling (Torrents, 2018)

As well as the Cold Plate, the in-wheel motor cooling block design aimed to reach the main objectives of this project: maximum weight reduction, minimum energy consumption and maximum reliability. This is why the following motor cooling block was presented: a nylon 3D-printed cooling block.

Compared to a typical aluminium motor case, its density was 3 times lower, and the manufacturing possibilities were much greater using 3D printing. In addition, it was capable of withstanding temperatures up to 200ºC without melting, as well as having a high HDT under different loads, making it the best substitute of a typical aluminium cooling block while achieving the main objectives of this project. There were other options for 3D printing (ABS and PLA), all of them thermoplastics that could fit for a cooling device, but due to their low HDT they were not suitable for this application (MakeItFrom, 2018).

More specifically, the material selected for this application was nylon HP 3D High Reusability PA 12 Glass Beans, manufactured by Hewlett Packard and composed by a polyamide containing a 40% of micro glass beans, considerably increasing its HDT. More information of the material may be found in Annex A.

Besides, the manufacturing process would require a Sodium Hydroxide bath in order to build the part, which is only suitable for 3D printed parts of nylon, rejecting the ABS and PLA's solutions.

In order to print the motor cooling block, a supporting material has to be added to the printed, needing a double-extruder 3D printer. The water circuit would be printed with PLA, whilst the remaining part of the cooling block would be nylon. Once the printing process is finished, a caustic soda bath is required in order to dissolute the PLA material and, at the same time, providing a smoother surface for the fluid channels.

Furthermore, other teams had already used this type of heat exchanger, as it can be seen in the following figure from the Norwegian University of Science and Technology (NTNU), seemingly proving it is as an effective design in Figure 5.5.

Figure 5.5 3D-printed motor cooling block design (Aune 2016).

On the other hand, according to design limitations a structural casing made out of aluminium had to surround the in-wheel motor. Figure 5.6 shows the 3mm thick aluminium structural case.

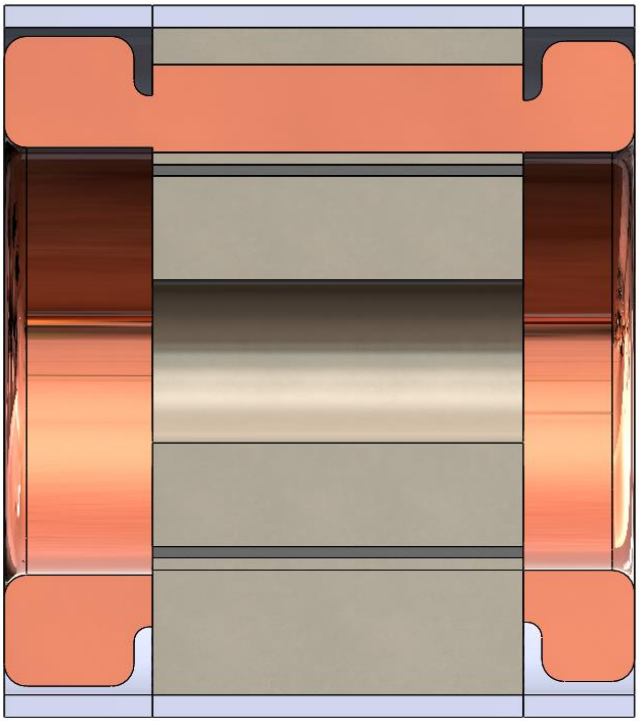

Figure 5.6 In-wheel motor CAD surrounded by the 3mm thick aluminium case.

6. Analytical study and geometrical configurations

Before carrying out any numerical calculation, analytical studies helped pre-dimensioning the whole cooling system. This indispensable step was accomplished by using the aforementioned equations in chapter 4 – heat transfer and fluid mechanics equations - awarding a first idea to the heat exchangers' design.

First of all, some assumptions had to be made, so heat transfer analysis could be simplified. It was assumed steady-state conditions, as well as fully developed fluid flow inside the water channels. Besides, water channels were assumed to be under constant surface heat flux and under constant surface temperature, so the temperature profiles remained constant.

6.1. Motor controller theoretical analysis

6.1.1. Inverters' maximum operating temperature

To start with, it was considered the inverter's cooling. The first approach was to study the maximum temperature that could be reached on the inverter's surface contacting the Cold Plate. By performing Eq. 4.2 with the maximum operating conditions imposed by the manufacturer, two possibilities appeared, depending on the thermal resistance of the assembly. An example is represented in Figure 6.1.

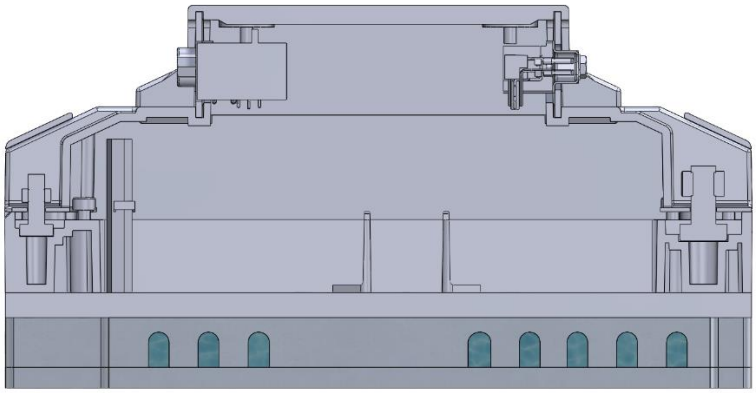

Figure 6.1 Motor inverter and Cold Plate assembly CAD cross-section representation.

As it may be seen in Figure 6.1, a thermal resistance appeared in-between the inverter and the Cold Plate. Applying Eq.4.2 with T_2=80ºC and $\dot{Q}$=300W:

$$\dot{Q} = \frac{\Delta T}{R} \rightarrow T_1 = T_2 - \dot{Q}R = 80 - 300R$$

The resulting T_1, which was considered the maximum allowed temperature on the connecting surface of the Cold Plate with the inverter, depended on the thermal resistance. According to the manufacturer, attaching the motor controller to an external N5 Cold Plate surface resulted in a thermal resistance of 0.07ºC/W between the inverter and the Cold Plate itself, while adding a thermal compound the thermal resistance could be as low as 0.03ºC/W. The results showed the importance of adding a thermal compound to reduce the maximum allowed temperature on the Cold Plate.

- Maximum working temperature without thermal compound $(R = 0.07ºC/W)$

$$T_1 = 80 - 300 \cdot 0.07 = 59ºC$$

- Maximum working temperature with thermal compound $(R = 0.03ºC/W)$

$$T_1 = 80 - 300 \cdot 0.03 = 71ºC$$

Adding a thermal compound allowed a greater maximum temperature of 71ºC on the connecting Cold Plate surface.

6.1.2. Mass flow rate and heat exchange area for the inverters

Then the mass flow rate and the heat exchange area for the heat sink were calculated using Eq. 4.6

$$\dot{m} = \frac{\dot{Q}}{C_p \Delta T} = \frac{300}{4190 \cdot (70 - 67)} = 0.0238\ kg/s$$

assuming 300W of heat losses, an exit and inlet temperature of 70ºC and 67ºC, respectively, and an average isobaric specific heat of 4190 J/kg·K. The outlet temperature was chosen according to the limit imposed by the maximum working temperature of the Cold Plate, 71ºC, and the temperature difference (3ºC) based on a global temperature difference of 10ºC between the Cold Plate and the motor cooling block, in order to take a first approximation of a radiator.

The heat exchange area came defined by Eq. 4.4 as

$$A_s = \frac{\dot{Q}}{h \Delta T_{ln}}$$

where the heat losses were 300 W and the logarithmic temperature difference 2.16ºC, according to Eq. 4.5. The remaining unknown parameter was the convection coefficient, which was calculated by using Eqs. 4.9, 4.14, 4.8 and 4.7:

$$Re = \frac{\rho c D_H}{\mu} \rightarrow f = \frac{1.325}{(ln\left(\frac{\varepsilon}{3.7D_H}\right) + \frac{5.74}{Re^{0.9}}))^2} \rightarrow Nu = \frac{\left(\frac{f}{8}\right)(Re - 1000)Pr}{1 + 12.7\left(\frac{f}{8}\right)^{0.5}(Pr^{\frac{2}{3}} - 1)} \rightarrow h = \frac{k \cdot Nu}{D_H}$$

By writing the results in Table 6.1, we obtained the following for some given characteristic diameters:

D_H (mm)	Mass flow rate (kg/s)	Fluid velocity (m/s)	Re	F	Nu	h (W/m²·k)	A (m²)	A (mm²)
3.00	0.0239	3.45	24651	0.0254	120	26311	0.00527	5269
6.00	0.0239	0.86	12326	0.0295	65	7086	0.01957	19565
9.00	0.0239	0.38	8217	0.0327	45	3272	0.04237	42367
12.00	0.0239	0.22	6163	0.0355	34	1871	0.0741	74104

Table 6.1 First approach of the convection coefficients and area needed to dissipate the inverters' losses.

This gave an idea of the required mass flow rate to dissipate the 300 W and the area needed. Though, the fluid velocity inside the heat sink would be, in most cases, unsuitable, since the fluid velocity must be between 1 and 3 m/s in order to avoid fouling inside the heat exchangers.

On the other hand, a mass flow rate and a hydraulic diameter had to be computed for the motor cooling block, so these were the first numbers obtained towards the final solution.

6.2. Motor cooling block theoretical analysis

In parallel, a first iteration of the motor cooling block water channel was carried out, following the same steps as in the motor controllers' heat sinks.

6.2.1. Maximum operating temperature for the motor cooling block

The maximum operating temperature came defined by the maximum temperature of the inverters, as well as the first radiator dimensioning. Therefore, with a global temperature drop of 10ºC, the maximum temperature that could be reached by the motor was firstly imposed to be 80ºC, with an inlet temperature of 70ºC – the outlet temperature of the Cold Plate – and outlet temperature of 77ºC – to accomplish the temperature drop of 10ºC.

In order to simplify the thermal management of the motor, the heat losses were assumed to be applied on the inner side of the aluminium structural case as seen in Figure 5.6, as well as the maximum operating temperature of it.

6.2.2. Mass flow rate and heat exchange area for the motor cooling block

By following the same procedure carried out with the inverters' heat sink – assuming 1210W of heat losses -, the results were obtained for the cooling block, written in Table 6.2.

D_H (mm)	Mass flow rate (kg/s)	Fluid velocity (m/s)	Re	f	Nu	h ($W/m^2 \cdot k$)	A (m^2)	A (mm^2)
6.00	0.0412	1.49	22750	0.0254	107	11738	0.0177	17731
5.00	0.0412	2.15	27300	0.0244	125	16527	0.0126	12593
4.00	0.0412	3.36	34125	0.0235	152	25188	0.00826	8262

Table 6.2 First approach of the convection coefficients and area needed to dissipate the motor's losses.

Since the structural aluminium case was 3mm thick, the heat transfer due to conduction was not taken into account. Therefore, the heat exchange area needed to dissipate the heat losses had to surround the aluminium case, cooling it down to the imposed values. Besides, all configurations were suitable due to the fluid velocity inside the system.

D_H (mm)	Mass flow rate (kg/s)	Fluid velocity (m/s)	Re	f	Nu	h ($W/m^2 \cdot k$)	A (m^2)	A (mm^2)
3.00	0.0412	5.96	42555	0.0229	193	42403	0.00327	3269
6.00	0.0412	1.49	21277	0.0258	104	11395	0.01217	12166
9.00	0.0412	0.66	14185	0.0283	73	5326	0.02603	26030
12.00	0.0412	0.37	10639	0.0305	56	3096	0.04478	44780

Table 6.3 Convection coefficients and area needed to dissipate the inverters' losses**.**

As it may be observed, different mass flow rates were obtained for both heat exchangers. It forced the calculations to choose a value between one of them, since the mass flow rate through the cooling circuit is always constant due to mass conservation. A first-approach value was chosen to be 0.0412 kg/s, the mass flow rate calculated from the motor heat losses.

Consequently, the mass flow rate and the required heat exchange area needed for the Cold Plate resulted to be the ones shown in Table 6.3.

According to the previous criteria, the water velocity should be between 1 and 3 m/s. Therefore, it was chosen a 6mm characteristic diameter for the Cold Plate water channel.

6.3. Geometrical models

Once the heat exchange area and mass flow rate needed to dissipate all the heat loses were calculated, geometrical iterations were drawn in order to carry out numerical analysis that could provide all the required data – pressure drops, temperatures and fluid velocities through the cooling devices – to design the cooling system.

By using CAD software, the water channels could be designed according to the heat exchange area previously calculated, which are shown in the following sections.

6.3.1. Cold Plate CAD models

As it was stated, the Cold Plate was to be decided between two different models, both differentiated by the manufacturing process: a drilled Cold Plate, which was thought to be the cheapest option, and a machined one, that could be optimized in pressure losses and weight.

6.3.1.1. Drilled Cold Plate

The drilled Cold Plate only contained drilling operations in an aluminium plate. The holes that did not cover the inside of the heat sink were covered with plastic taps, as it is shown in Figure 6.2.

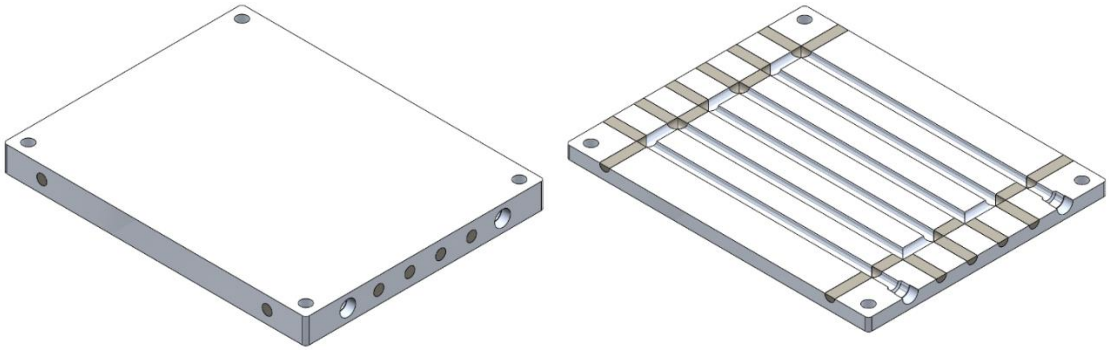

Figure 6.2 Drilled Cold Plate configuration and a cross-section representation. Plastic taps are represented in brown colour.

According to the analytical calculations, the water channel area had to be equal or greater to the calculated area. In this case, the heat exchange area was 17813 mm^2, a 46% greater than the needed area and weighted 928g.

6.3.1.2. Machined Cold Plate

This model was a machined Cold Plate, which design was based on the last season's Cold Plate. It was composed by the Cold Plate itself and an aluminium cover under it, shown in Figure 6.3.

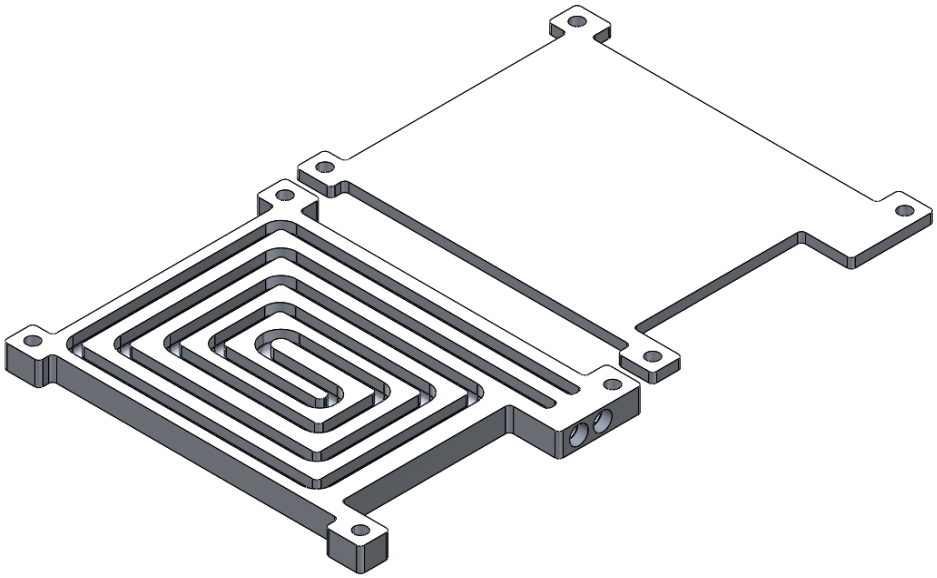

Figure 6.3 Machined Cold Plate configuration and its cover.

In this model, the heat exchange area was greatly superior to the area analytically calculated - 34373 mm^2, a 93% larger than the required area. Despite of that, it was important to take into account the surface distribution along the heat sink. This is the reason why the water channel area was that large and was located in that place. Besides, the weight reduction was considerably increased – total Cold Plate weight of 717g, a 22% less. However, a stress analysis should be carried out to validate the design in order to have a mechanically functional heat sink, which was not included in this project scope. All of this is summarised in Table 6.4, where the area extension – the area amount which surpasses the theoretically needed area – and mass for each configuration is given.

Both models presented and M5 hole in each corner, needed to fix the Cold Plate to the motor controller and a 1/8 NPT hole in the inlet and outlet holes, since they were required in order to attach a connector that could fit a hose fitting – needed to physically connect the heat sink to the cooling system. It is important to note that the minimum thickness of the heat sink came imposed by the fitting connectors' holes. So, these were the initial configurations that allowed the first numerical analysis of the thermal devices.

Configuration	Area extension (%)	Mass (g)
Drilled	46	928
Machined	93	717

Table 6.4 Comparison between the drilled and machined Cold Plate.

6.3.2. Motor cooling block models

The motor cooling block was to be designed as a nylon 3D printed heat exchanger with a helix water channel around the aluminium case. One of the most important design parameters that was taken into account was the number of revolutions the water channel would do around the motor, since it would determine the amount of heat exchange area.

The model prepared for the motor cooling block satisfied the analytical calculations previously done. With a similar characteristic diameter, the needed and designed heat exchange area were presented in Table 6.5.

Config.	Length (mm)	Height (mm)	D_H (mm)	A (m^2)	A (mm^2)	Area CAD (mm^2)	Area difference (mm^2)
A	8	5	6.33	0.01961	19606	24273	4667
B	8	4	5.50	0.0150	15037	22112	7075
C	8	3	4.50	0.01033	10331	19988	9657

Table 6.5 Heat exchange area for the 3 turns model.

The water channel configurations presented a rounded-square profile around the motor case with a radius of 0.5mm. Case A was the tallest profile with a height of 5mm, while case C, the smallest with 3mm. Sketch of case A can be seen in Figure 6.4.

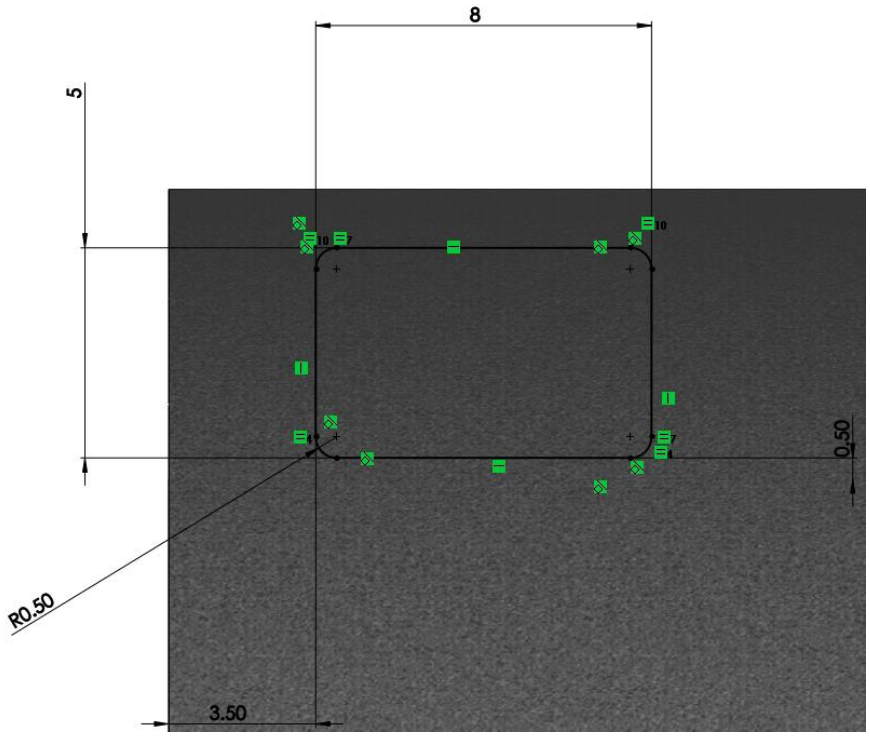

Figure 6.4 Sketch of the configuration A water channel around the motor case.

In order to properly visualise the water channel, Figure 6.5 and Figure 6.6 show the external view of the motor cooling block. It was a helix surrounding the motor case with 3 revolutions around it. However, due to the low thermal conductivity of nylon, it was predicted that the hand-made calculations were not properly accurate. Therefore, a second model was proposed with identical configurations but with 8 revolutions around the motor case. Both models are presented in Figure 6.6.

Figure 6.5 Motor cooling block external view

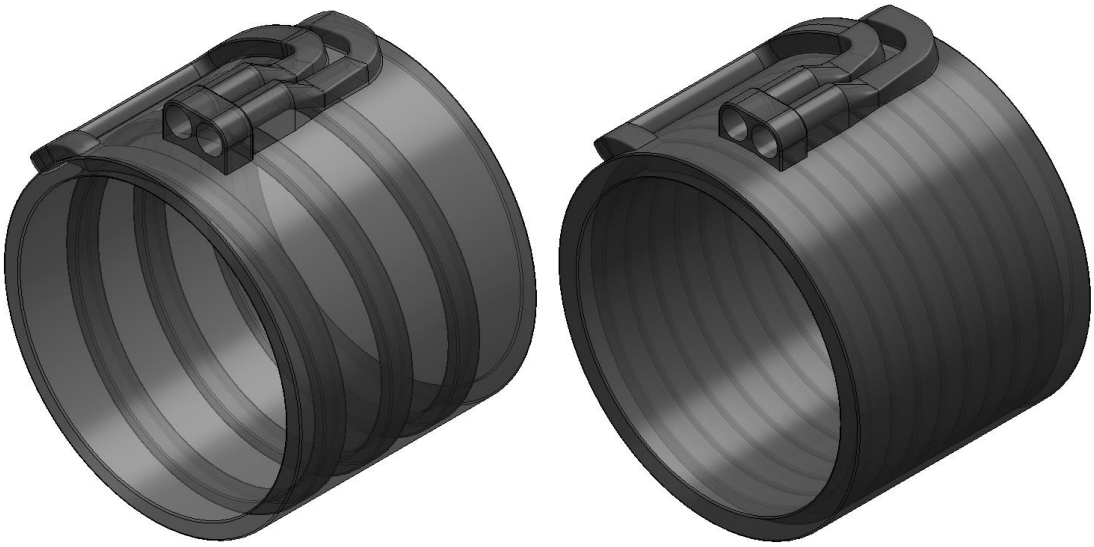

Figure 6.6 Motor cooling block water channel's 3 and 8 turns models at the left and right zones, respectively.

Despite having a much larger heat exchange area than the calculated one, it was predicted to have a better performance than the 3 revolutions one due to the low nylon's thermal conductivity. These configurations may be observed at Table 6.6, having all the water channels the same profile than in the 3 revolutions model.

Config.	D_H (mm)	A (m^2)	A (mm^2)	Area CAD (mm^2)	Area difference (mm^2)
A2	6.33	0.01961	19606	70418	50812
B2	5.50	0.0150	15037	64512	49474
C2	4.50	0.01033	10331	58412	48080

Table 6.6 Heat exchange area for the 8 turns model.

7. Numerical analysis

A numerical analysis of the cooling system was only applied to the Cold Plate and Motor cooling block. Neither the radiator nor the pump systems were modelled, since they were analysed by other methods. Therefore, the numerical analysis of the cooling system was split into three different parts: pre-processor, solver and post-processor. As so, in this chapter was described the pre-processing part since the solver used has already been explained in section 4.2. Post-processing was analysed in the results section.

7.1. Pre-processing

Pre-processing was mainly composed by the following parts: definition of the geometry of the region of interest – computational domain; grid generation; selection of the physical phenomena needed to be modelled and definition of fluid properties and specification of appropriate boundary conditions at cells that touch the domain boundary - (Versteeg, Malalasekera, 2007).

7.1.1. Computational domain and boundary conditions

7.1.1.1. Cold Plate

For this case, two different computational domains were taken into account as a result of the two Cold Plate models. Both of them were composed by the aluminium heat sink itself and the water domain.

7.1.1.1.1 Drilled Cold Plate domain

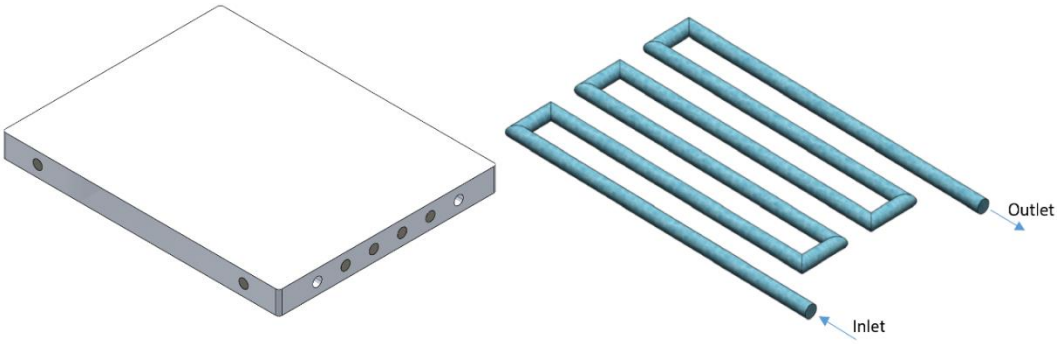

Figure 7.1 Drilled Cold Plate and water domain. The fixing holes disappeared and the connecting holes at the inlet and outlet, simplified.

At the heat sink was assumed a heat source at the upper surface of 300W – the surface that was in contact with the inverter's surface -, according to the inverter's heat losses and an initial temperature of 67ºC for the whole domain – heat sink and water. The computational domain was slightly different from the original model as it is shown in Figure 7.1, as well as the water domain.

And at the water domain two different boundary conditions were assigned: a mass flow inlet and a pressure outlet that might be appreciated in the same figure. The mass flow rate was chosen to be 0.0412 kg/s and at 67ºC, as it was previously established.

7.1.1.1.2 Machined Cold Plate

The boundary conditions remained the same for the whole domain – heat sink and water. Figure 7.2. shows the machined Cold Plate, which actually did not have fixing holes likewise the drilled Cold Plate, and the water mass flow inlet and pressure outlet surfaces.

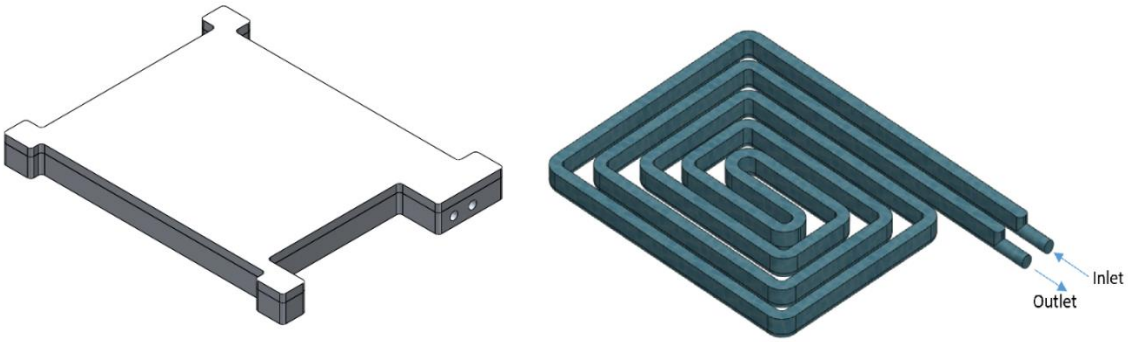

Figure 7.2 Machined Cold Plate domain.

7.1.1.2. Motor cooling block and aluminium case

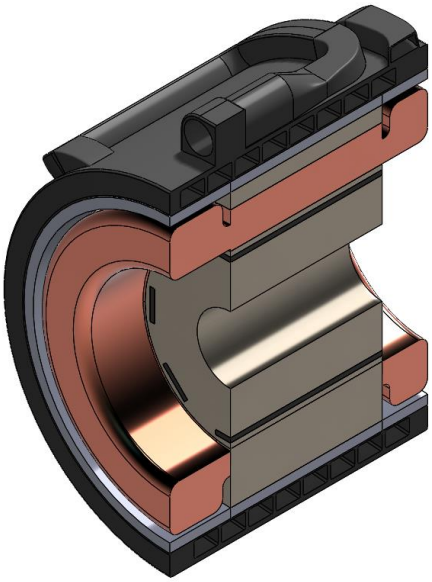

Figure 7.3 Motor cooling block and motor cross-section representation.

The computational domain for the motor cooling block was already stated in Figure 6.5 and there is only one boundary condition, applied to the outer surface of it: heat transfer due to air-forced convection. As the cooling case is an in-wheel motor case, some air flows around the outer surface of

the motor case. It was selected a 10W heat transfer from the cooling block to the air. An assembly of the motor cooling block and the aluminium case is represented in Figure 7.3.

For the water domain, the boundary conditions are equal than in the Cold Plate fluid modelling: a mass flow rate of 0.0412 kg/s at the inlet but at 70ºC and a pressure outlet, as it might be seen in Figure 7.4.

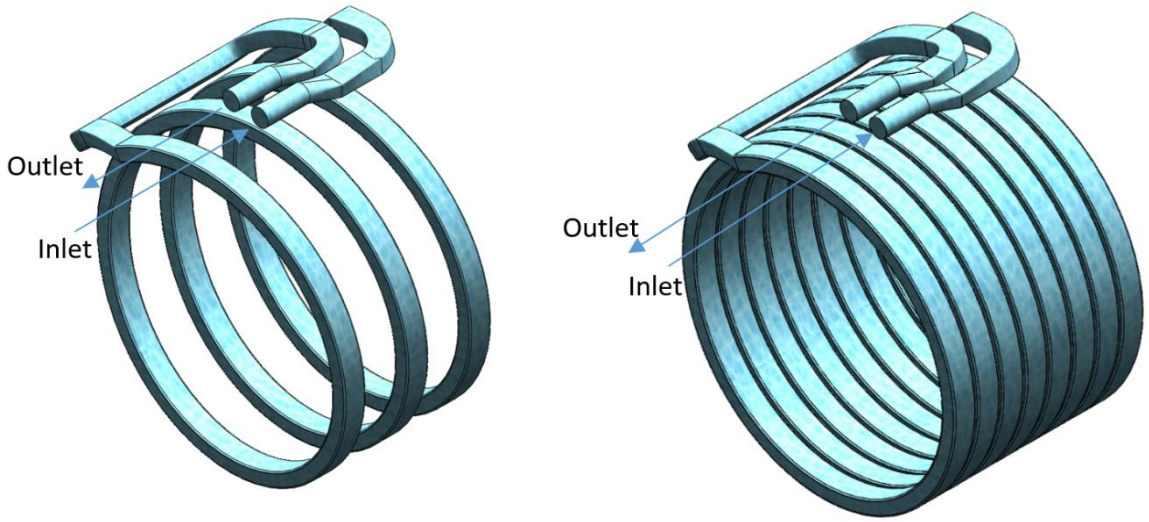

Figure 7.4 Water domain and boundary conditions for the motor cooling block models.

The aluminium case was a simple aluminium cylinder, which was virtually divided into three different parts: the shield case, the centre or stator case and the flange case. This was due to the different heat losses inside the electric motor, as defined in section 3.2.1. A better representation of the aluminium case can be seen in Figure 7.5.

In order to proceed with the numerical analysis and to properly assign the correct boundary conditions to the solid domain, this was divided into the aforementioned parts. Hence, the heat losses were assigned to each part inner surface according to each surface area and power losses. These power losses were divided as: winding losses, iron losses, mechanical losses, rotor losses and additional losses. The total losses distribution is shown in Table 7.1.

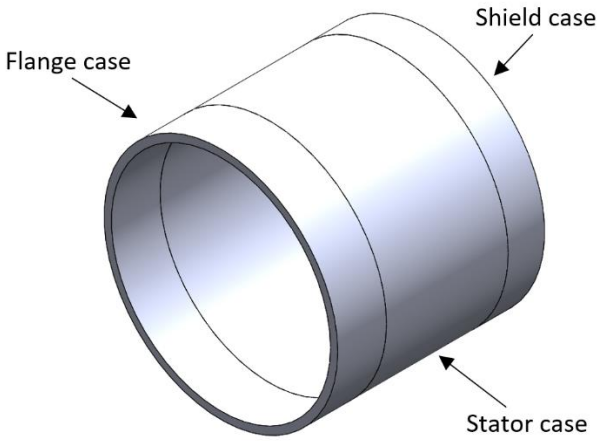

Figure 7.5 Structural aluminium case virtual division.

Aluminium losses distribution	Area (mm^2)	Area (%)	Winding losses (W)	Iron losses (W)	Mechanical losses (W)	Rotor losses (W)	Additional losses (W)	Total losses (W)
Stator case	14137.17	58.82	156.73	821.74	0	9.93	66.67	**1055.07**
Shield case	5654.87	23.53	62.69	0	22.96	0	0	**85.65**
Flange case	4241.15	17.65	47.02	0	22.96	0	0	**69.98**
Total aluminium case	24033.19	100	266.44	821.74	45.92	9.93	66.67	**1210.70**

Table 7.1 Motor losses distributed on the inner face of the aluminium case according to its virtual division.

7.1.2. Grid generation

The discretization of the computational domain allowed the calculations of the mass conservation, linear momentum and energy equations in order to find the required data. In general, the more elements the domain contains, the more accurate the solution is. However, any numerical calculation implies numerical errors, conducting to a non-perfect solution. Eventually, as the number of elements increases, the results obtained do not depend on the mesh decomposition. As a consequence, there is a number of elements in the grid domain that defines the maximum result's resolution, where taking more elements would not result in more accuracy.

For this reason, is necessary to find a grid which is independent of the number of mesh elements. As so, a grid independence study was carried out for both cooling devices.

7.1.2.1. Grid independence study: Cold Plate

One of the most important parts of the mesh generation is the near wall region mesh. In a turbulent regime, the boundary layer does not behave in the same way as in a laminar flow.

Walls are a source of vorticities, and they must be analysed in order to ensure an accurate solution. Thus, a precise near wall region study determines a successful prediction of wall bounded turbulent flows. A very common parameter used to model this region near the wall is called y^+, which is a non-dimensional number used to define the boundary layer regions for turbulent regimes. It may be written as

$$y^+ = \frac{y u_\tau}{\upsilon} \qquad \textbf{(Eq. 7.1)}$$

where y is the distance normal to the wall, u_τ is the friction velocity and υ the kinematic viscosity of the fluid. At the same time, the friction velocity might be written as

$$u_\tau = \sqrt{\frac{\tau_\omega}{\rho}} \qquad \textbf{(Eq. 7.2)}$$

where τ_ω is the wall shear stress and ρ the fluid density.

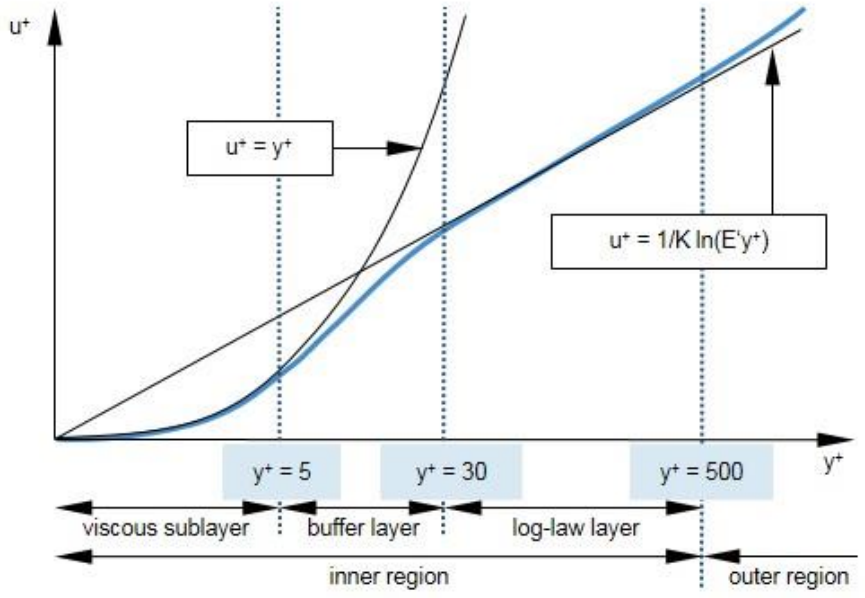

Figure 7.6 Different boundary layer regions for turbulent flows (Star-CCM+ Documentation).

To better represent the parameter effectiveness, it is generally plotted the variation of the so-called non-dimensional velocity u^+ against y^+ (Figure 7.6). For turbulent flows, the inner region of the

boundary layer can be divided into three sublayers: the first one, the viscous sublayer, where the viscous forces are predominant against the turbulence flow and requires a $y^+ < 5$; the second one, called the logarithmic area, where the turbulence stresses dominate the flow and velocity does no vary too much along distance y, where $30 < y^+ < 500$ and the last one, the buffer layer, where $5 < y^+ < 30$. The buffer layer is the transition region between the viscosity-dominated region and turbulence-predominant part of the flow.

As it was stated in section 4.2.4.3, the SST K-Omega turbulence modeller was chosen sue to its capability to analyse the viscous sublayer in the boundary layer region. So, as the turbulent flow parameters are dependent on the boundary layer, the grid independence study also depended on it.

Instead of making a grid independence study for each configuration of each Cold Plate and motor cooling block model, it was analysed only one model for each cooling device. The reason to do that was due to the flow regime and boundary conditions of each case: they were identical. Besides, it was taken a configuration which would guarantee the highest Re number of all configurations in each model. This would induce to the thinnest boundary layer of each cooling device. Consequently, if this configuration were grid independent, all the remaining configurations would be independent too.

To sum up, to accomplish the mesh independence study, it was necessary to find out a mesh density in the fluid domain of each cooling device's configuration, as well as in the solid domains.

The proposed geometry for the grid independence study was a similar model than the machined Cold Plate but easier to discretise, shown in Figure 7.7.

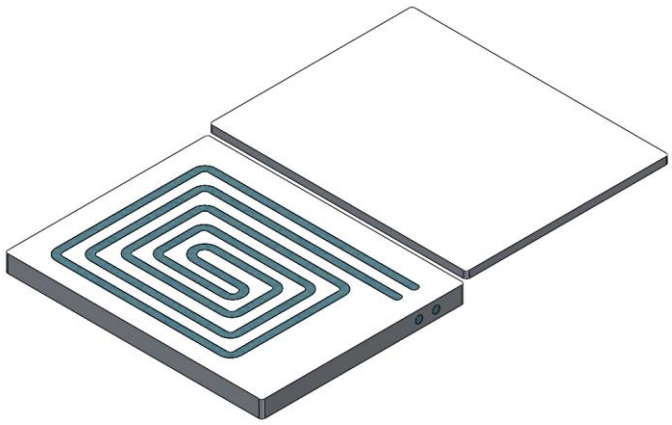

Figure 7.7 Grid independence Cold Plate domain (heat sink, water and cover).

Finally, the element type was chosen to be polyhedral, since it was more adaptable to non-regular geometries and more efficient in terms of number of elements than tetrahedral or hexahedral elements.

7.1.2.1.1 Cold Plate fluid domain

For the fluid domain, the objective solution variable was the pressure drop across the water channel. Besides, it was ensured that the mass and energy were conserved.

The computational domain, shown in Figure 7.7, includes a velocity inlet of 3 m/s and a pressure outlet, that together with a characteristic length of 8.52 mm, resulted in a Re number of 62200, much greater than in all the actual study configurations. The fluid volume was of 90141 mm^3.

Given the computational domain and the boundary conditions, it was simulated a fluid flow analysis for the water domain. The results showed a fluid domain with several vorticities which are unsteady in nature. As a consequence, an unsteady analysis was needed, since a steady study could not capture the vorticities due to boundary layer separation and the errors were considerable. Both analysis represented in Figure 7.8 and Figure 7.9, respectively.

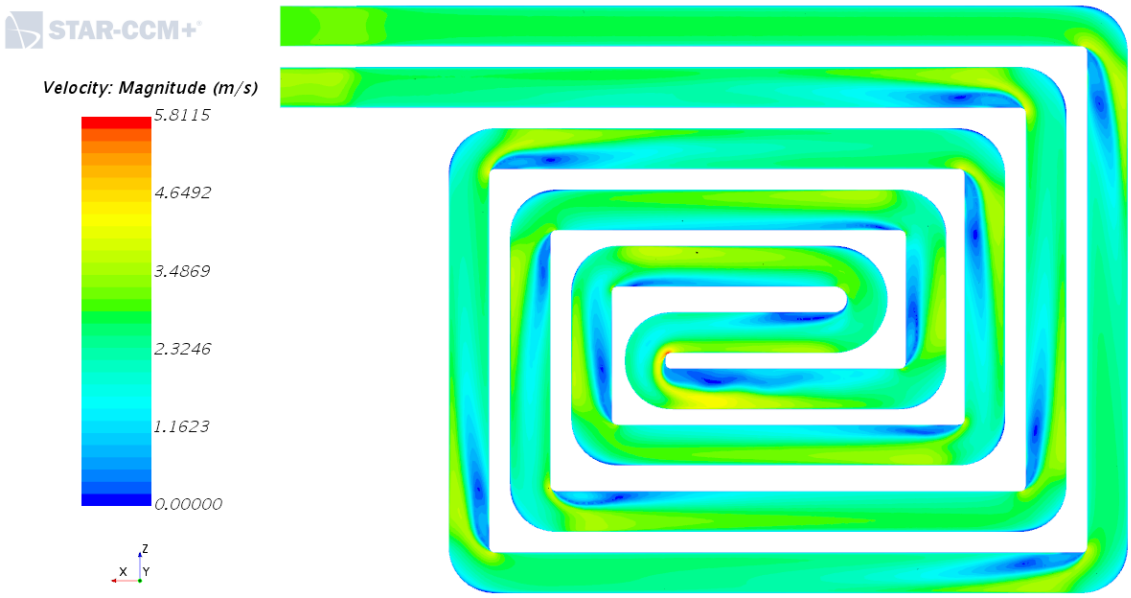

Figure 7.8. Velocity contours of the first steady state fluid domain simulation.

For an unsteady state simulation, a time step had to be chosen. This selection was carried out using the Large Kolmogorov characteristic scales, declaring the fluid velocity and characteristic length, a time-step of 0.00284 s was selected (Versteeg, Malalasekera, 2007).

So the procedure was to carry out a steady simulation until convergence was achieved. Then, a second order temporal discretization was implied in an unsteady state simulation, until the residual errors decreased and converged in a virtual time of 3 seconds.

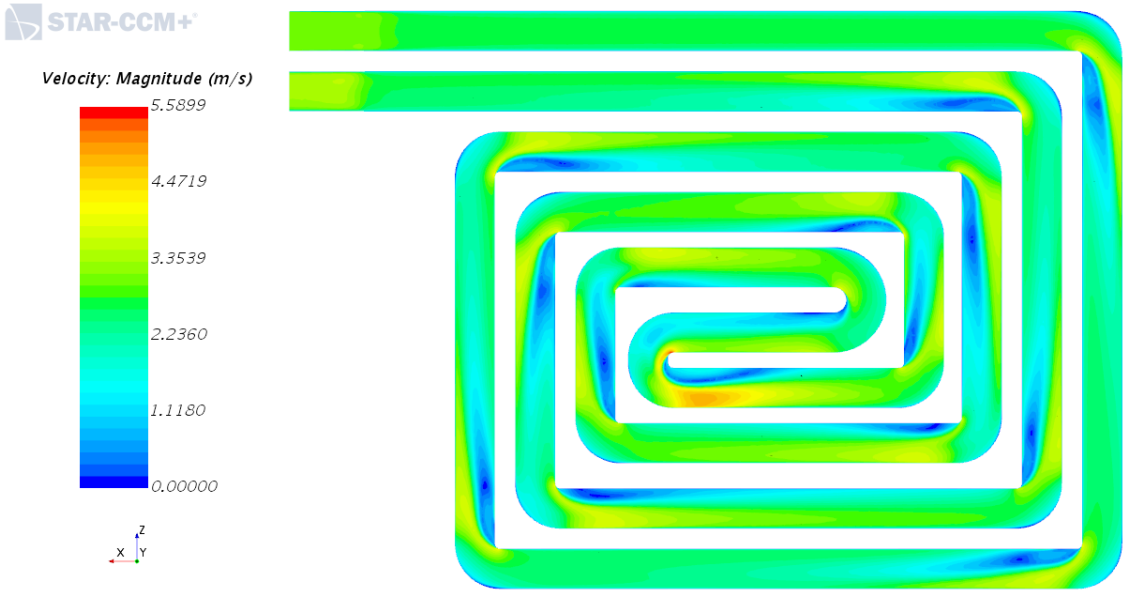

Figure 7.9 Velocity contours of the unsteady state fluid domain simulation.

Then, for different number of cells, the grid independence study, for an initial value of y^+=1, the results were the ones shown in Table 7.2 and Figure 7.10.

Number of cells	Mesh density (cells/mm^3)	Pressure drop (Pa)	Meshing time (s)	Er (%)
664375	7.37	36790	130.11	8.56
944196	10.47	36601	144.31	9.03
1293944	14.35	38689	163.68	3.84
1733179	19.23	38300	200	4.81
1898425	21.06	38490	214.09	4.34
2170035	24.07	39941	247.19	0.73
2383173	26.44	39827	266.21	1.01
2897970	32.15	40235	330.83	-

Table 7.2 Results of the mesh independence study of the Cold Plate's fluid domain.

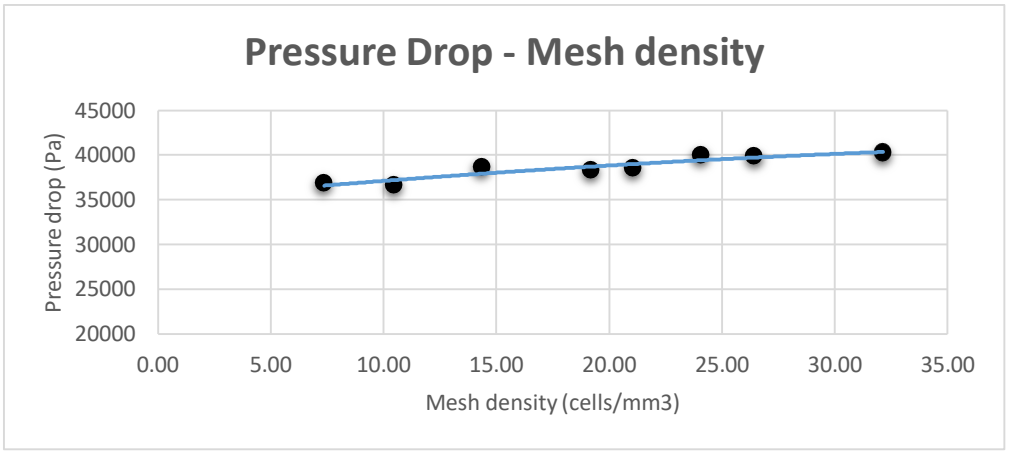

Figure 7.10 Pressure drop against mesh density plot for the grid independence study of the Cold Plate's fluid domain.

For coarser meshes, the boundary layer separation was not included, resulting in a lower pressure drop. The selected mesh density was 24 cells/mm^3, since it only differed less than a 1% from the converged solution. Moreover, it was carried out an independence study with respect to the y$^+$ parameter, represented in Table 7.3.

y+	Prism layer near wall thickness (m)	Pressure drop (Pa)	Mass conservation (kg)	Er (%)
200	9.75E-04	29420	7.59E-07	26.34
100	4.87E-04	29236	1.62E-09	26.80
60	1.33E-04	39951	3.65E-08	0.03
5	2.44E-05	39695	1.40E-09	0.62
1	4.87E-06	39941	2.02E-08	-

Table 7.3 Results of the mesh independence study regarding the y+ values for the Cold Plate's water domain.

As the y$^+$ values increased, the pressure drop decreased, as it was expected. It was chosen a y$^+$ value of 60, since it provided almost the same results with less cells. The whole mesh is shown in Figure 7.11.

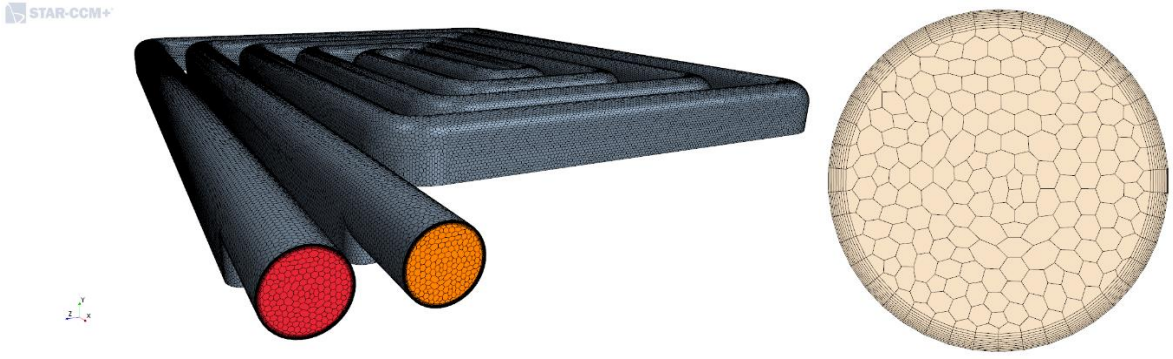

Figure 7.11 Mesh of the fluid domain with the final mesh density and y+ prism layers.

7.1.2.1.2 Cold Plate heat sink domain

This domain was easier to calculate than the fluid one. A random convection coefficient inside the water channel of 2500 W/m^{2}k and the heat source of 300 W in the contact face between the heat sink and the inverter. By using the same mesh element, the results were collected in Table 7.4 and Figure 7.12.

Number of cells	Mesh density (cells/mm^3)	T (ºC)	Meshing time (s)	Er (%)
471665	1.36	44.342	264.27	-
295255	0.85	44.342	180	0.001
262536	0.76	44.341	153.07	0.003
159281	0.46	44.339	84.65	0.007
145688	0.42	44.333	88	0.021

Table 7.4 Results of the mesh independence study for the heat sink.

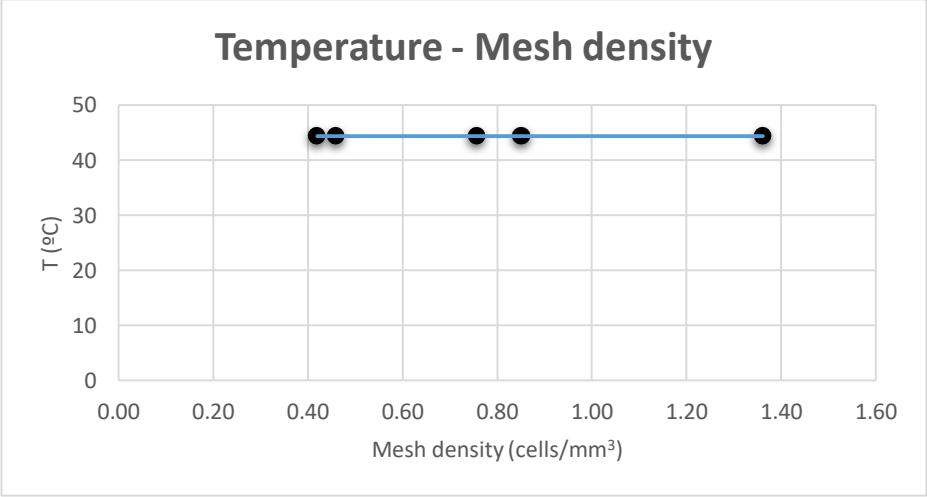

Figure 7.12 Temperature against mesh density plot for the grid independence study of the heat sink.

It was chosen a mesh density of 0.46 cells/mm^3 because it offered a great quality mesh while capturing the whole geometry of the heat sink. Coarser meshes did not capture the full geometry.

7.1.2.2. Grid independence study: Motor cooling block

7.1.2.2.1 Motor cooling block fluid domain

For the motor cooling block, the same exact procedure was followed. In this case, instead of using a different configuration for the mesh independence study, it was used configuration C of the 8 revolution model with an inlet velocity of 3 m/s. This resulted in a Re of 34300.

It was observed that the boundary layer separation phenomenon did not occur in this fluid flow. As a result, it was only calculated a steady state simulation with the aforementioned boundary conditions, represented in Table 7.5 and Figure 7.13.

Number of cells	Mesh density (cells/mm^3)	Pressure drop (Pa)	Meshing time (s)	Er (%)
32495243	482.40	134233	4645.00	-
15274142	226.75	134101	1399.86	0.10
10191727	151.30	133750	961.93	0.36
9736795	144.54	132567	674.87	1.24
7260903	107.79	129740	489.39	3.35
5343391	79.32	127784	482.82	4.80
1371433	20.36	123584	157.75	7.93
837164	12.43	126118	128.63	6.05

Table 7.5 Results of the mesh independence study of the cooling block's fluid domain.

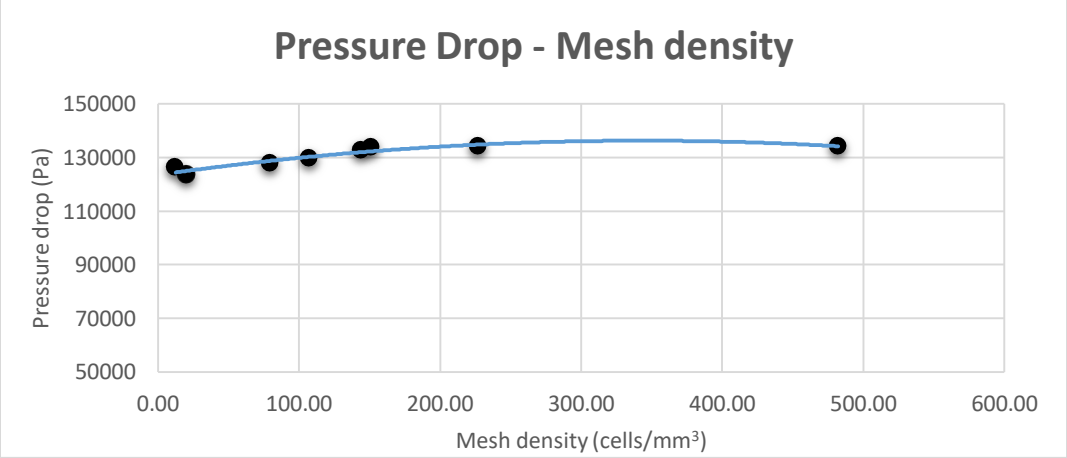

Figure 7.13 Pressure drop against mesh density plot for the grid independence study of the cooling block's fluid domain.

The resulting mesh density was to be chosen taking into account the y^+ values, as well as in the Cold Plate configuration.

y+	Prism layer near wall thickness (m)	Pressure drop (Pa)	Er (%)
1	4.56192E-06	133750	-
5	2.28096E-05	135920	1.62
60	0.000273715	182675	36.58
100	0.000456192	168006	25.61
200	0.000912383	210780	57.59

Table 7.6 Results of the mesh independence study regarding the y+ values for the motor's fluid domain.

Therefore, it was selected a mesh density of 151 cells/mm^3, according to the relative error statement imposed earlier and a y^+ of 5. Although the relative error was greater than a 1%, the number of cells was severely reduced to 4209000 cells, where less than a 50% of the cells were needed and thus decreasing the computational source required.

Besides, some areas of the fluid domain contained different mesh sizes due to the geometrical shapes. This and the final y^+ resolution might be noticed in Figure 7.14.

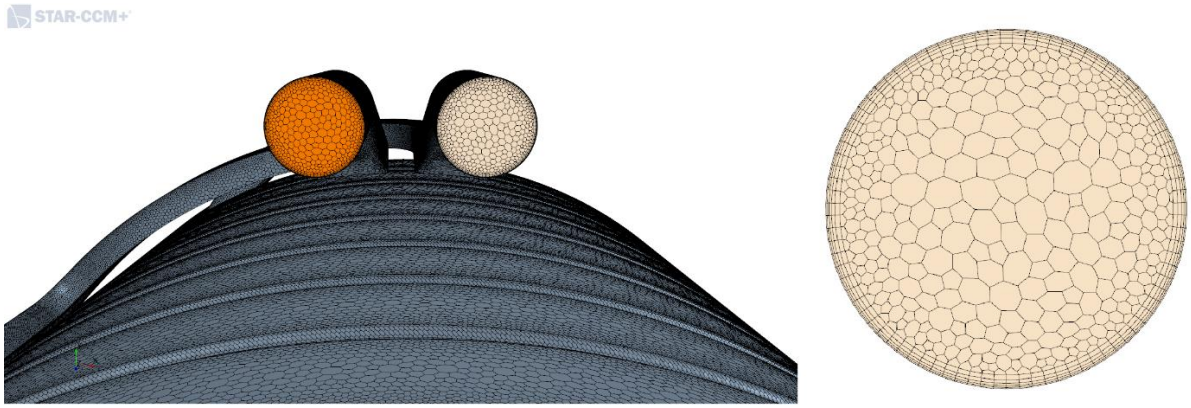

Figure 7.14 Fluid and boundary layer mesh for the motor's fluid domain.

7.1.2.2.2 Motor cooling block and aluminium structural case domain

Finally, the solid domains followed the same process as the Cold Plate's domain with the same boundary conditions. However, as the motor cooling block's cases were almost equal between them, the mesh independence was chosen by the number of cells, not the mesh density, as it can be seen in Table 7.7, Figure 7.15.

Number of cells	T (ºC)	Meshing time (s)	Er (%)
710320	89.14	455.73	0.11
719813	89.14	460.00	0.11
4116187	89.23	2384.80	-

Table 7.7 Results of the mesh independence study of the cooling block's domain.

Just a few studies were carried out for the cooling block and aluminium case, since less cells would not capture the entire geometry and more cells would not determine more accuracy. The mesh element selection for the aluminium case is represented in Figure 7.16 and Table 7.8.

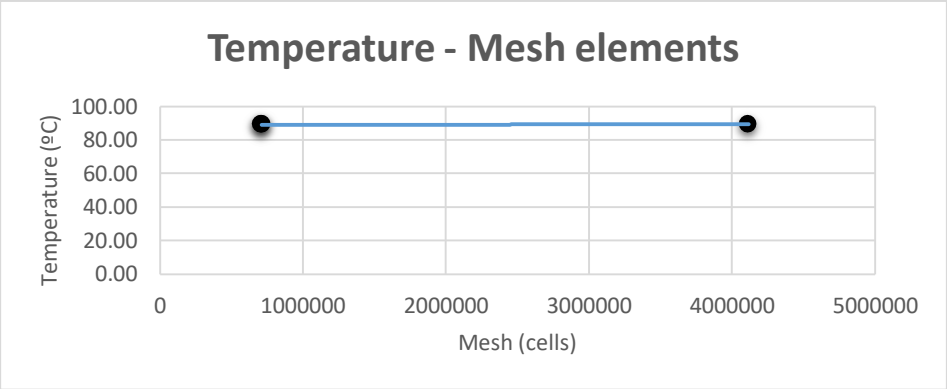

Figure 7.15 Temperature against mesh elements plot for the cooling block's domain.

Number of cells	T Max (ºC)	Er (%)
14339	69.672	0.02
32260	69.664	0.01
91017	69.659	-

Table 7.8 Results of the mesh independence study of the structural aluminium domain.

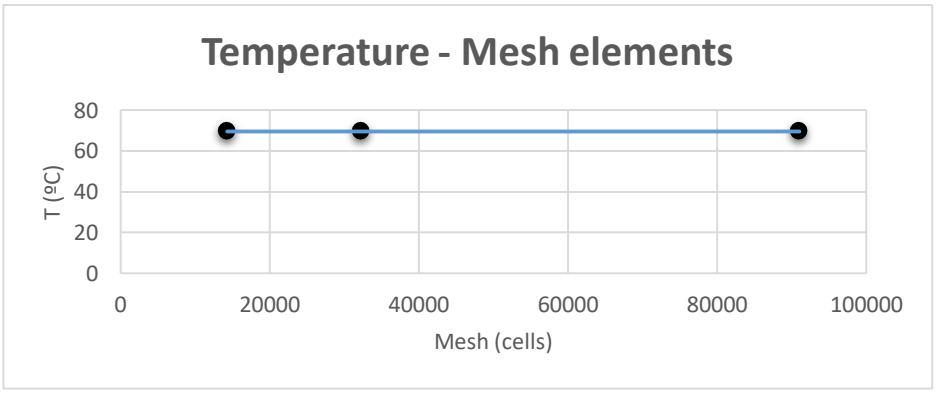

Figure 7.16 Temperature against mesh elements plot for the structural aluminium' domain.

Some refinements had to be done in order to capture the initial geometry of the heat exchanger. Specifically, in the upper part of the water channels, as well as in the inner fillets of the circuit.

7.1.3. Physical phenomenon and fluid properties definition

The physics applied to this computational domain were split into two parts in all cooling devices: the solid and the fluid regions. The solid regions would be aluminium for the Cold Plate and the structural case, plastic for the taps and nylon for the motor cooling block. On the other hand, the fluid domain would be water, with its physical properties depending on the cooling device – due to the average temperature of water inside them.

The physical properties of the Cold Plate and motor cooling block regions – solid and fluid - are presented in Table 7.9. To measure the water physical properties, it was taken into account the average

temperature of the fluid inside each heat exchanger – 68.5ºC in the Cold Plate and 73.5ºC in the motor cooling block, according to the boundary conditions already stablished.

The physical models selected for the fluid domain were the same for both heat exchangers. It was a three dimensional steady state liquid fluid, assuming constant density in a turbulence regime, where the turbulence model selected was SST K-Omega. Besides, it was used a segregated solver, which would not require much computational resources as a coupled solver. Meanwhile, the energy equation had to be solved, enabling a ''Segregated Fluid Temperature'' model. On the other hand, the wall treatment was selected to be a hybrid wall modelling that could behave well for low and high y^+ values, called ''All y+ Wall Treatment''. A screenshot of the physical models selected for the fluid domains might be observed in Figure 7.17.

Physical property	**Aluminium**	**Plastic**	**Nylon**	**Water (Cold Plate)**	**Water (Motor cooling block)**
Density (kg/m^3)	2700	1020	1040	978.60	975.70
Thermal conductivity (W/m·k)	183	0.23	0.30	0.659	0.661
Specific heat (J/kg·K)	870	2100	1740	4190	4200
Dynamic viscosity (Pa·s)	-	-	-	0.000411	0.000384
Prandtl number	-	-	-	2.61	2.44

Table 7.9 Physical properties for the Cold Plate and cooling block regions.

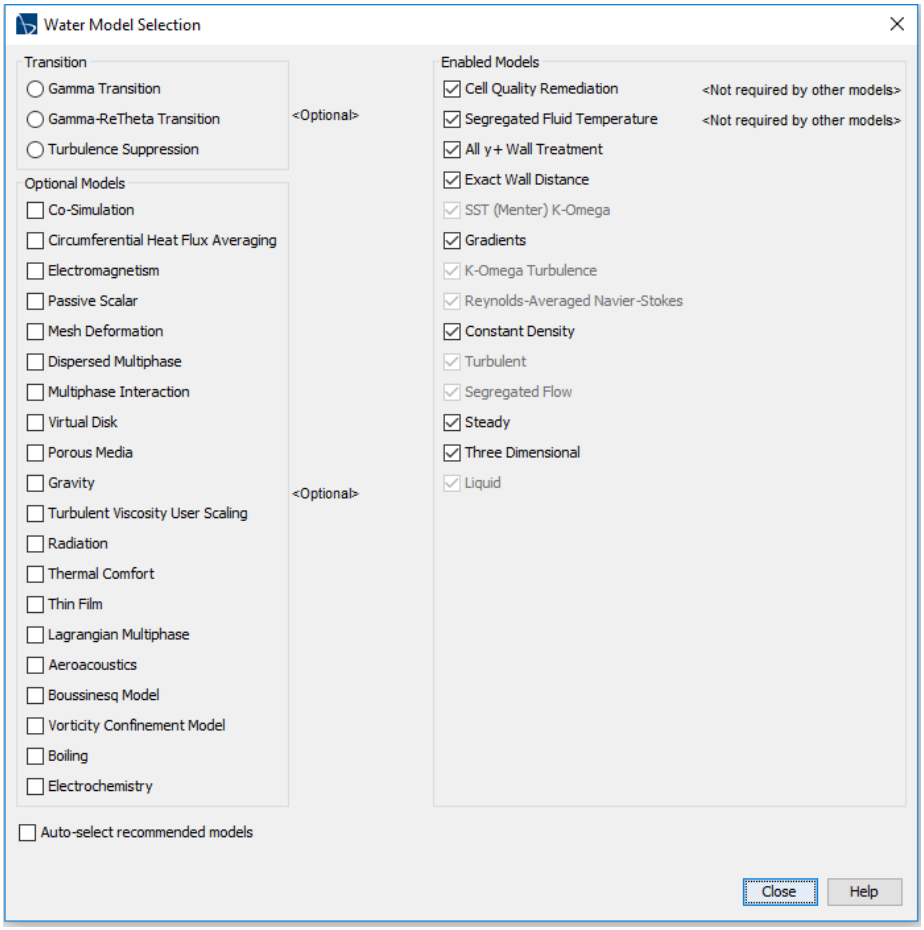

Figure 7.17 Physical models selected for the fluid regions.

8. Radiator experimental analysis

As it was explained in section 6.4.1, the radiator could not be selected analytically, since physical dimensions of the heat exchangers were not given by the manufacturers – fin density and exact geometry. Therefore, it was carried out an experimental test with last season's radiator in order to know if it was capable of exchanging enough heat to cool down the powertrain system.

The tested radiator was manufactured by Setrab, a Swedish company which designs and manufactures aluminium heat exchangers for the automotive industry. In this case, it belonged to the STD line, more specifically STD116, which was characterised by having 16 rows to transport the fluid and measured 210x122x50 mm, seen in Figure 8.1. So, to prove the radiator performance, an experimental test was needed. The objective was to determine the required area to dissipate the inverter's heat losses.

Figure 8.1 Setrab's radiator STD116 and its corresponding connectors.

The general setup of the experiment might be seen in Figure 8.3. It mainly consisted of the configuration of two fluids around the heat exchanger: air and water. The air was forced to circulate through the radiator by a two-speed fan, while water was pumped through it in a closed hydraulic circuit. More specifically, the radiator testing presented the following items: a plastic tank where water was stored and was used as the inlet and outlet of the circuit; a thermal resistance of 1400W to heat the water; silicone hoses, to transport the fluid; a water electric pump; an AC/DC current converter in order to supply 20V to the pump; a potentiometer, which allowed a variable current to the motor's pump; a data sensor, to register all the thermal data; the temperature sensors; an anemometer to measure air velocities and a two-speed fan.

In order to better visualise the experimental setup, Figure 8.2 represents a basic perspective of it.

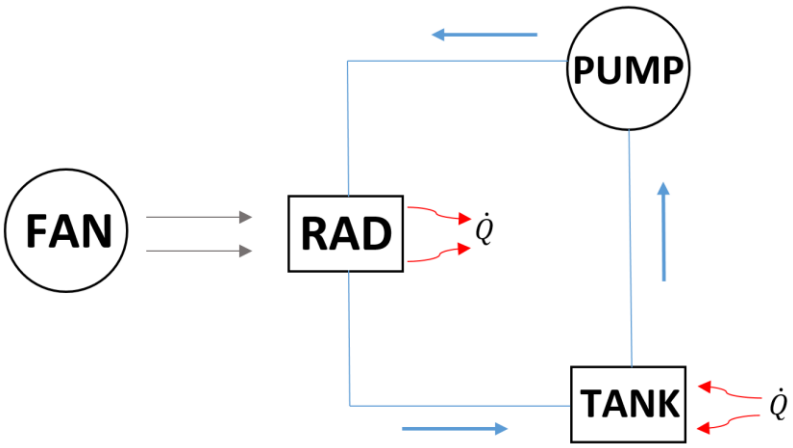

Figure 8.2 Basic schematic of the experiment setup.

The key point was to measure temperatures at both inlets and outlets of the heat exchanger: air and water. With these data collected, it was possible to measure the radiator performance. In order to do so, different volumetric flow rates were needed for the water side, as well as for the air side. Fan speed was directly controllable by making a simple electric schematic change inside the device, whilst the water pump volumetric flow rate was altered by feeding the motor's pump with different voltage values, done by a potentiometer which allowed a manual change of it. In the case of the water volumetric flow rate, the measurements were taken by gravimetric measures, where a deposit of 2L was filled and the time needed to do it was measured with a chronometer. On the other hand, the air volumetric flow rate was simply measured with the anemometer.

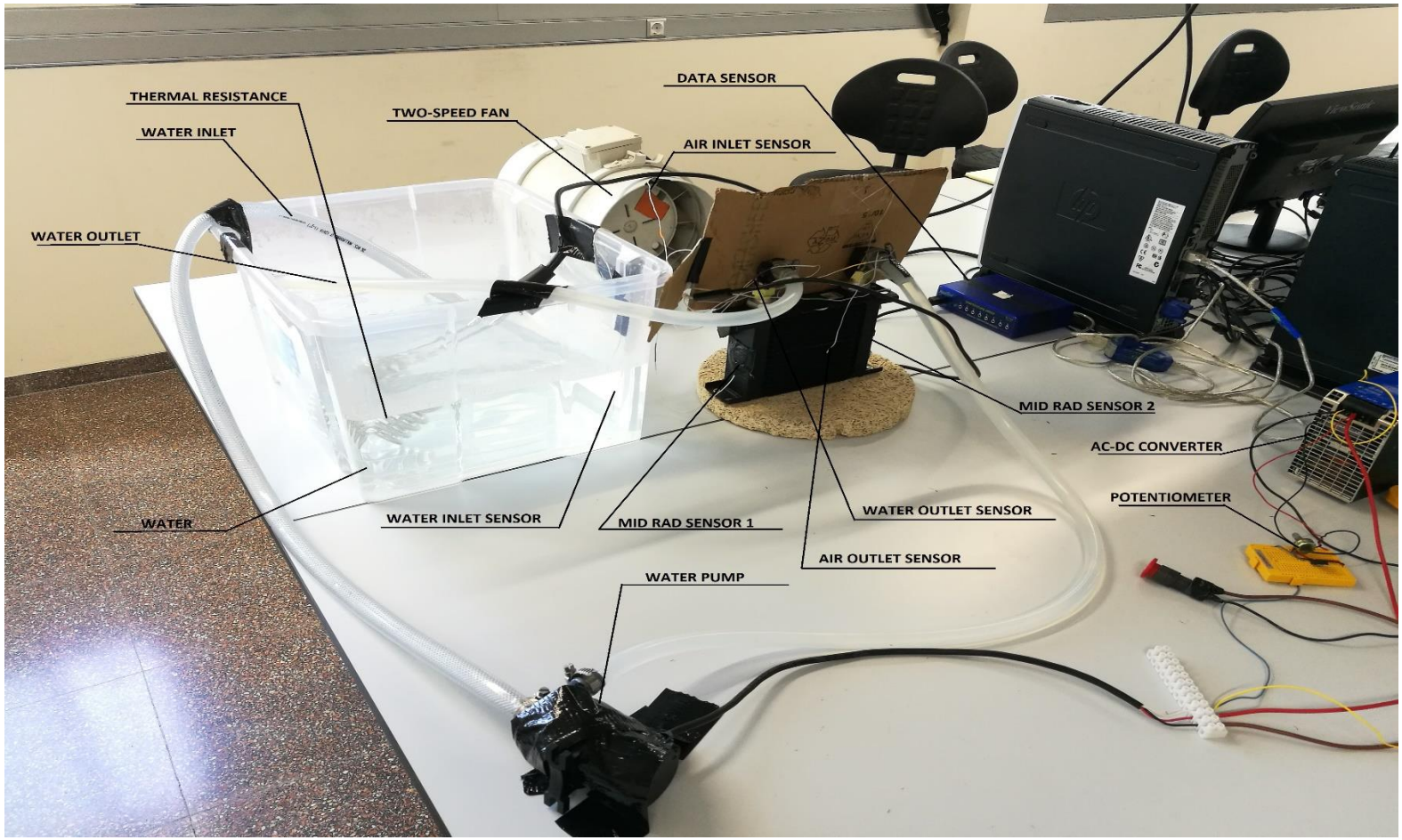

Figure 8.3 General setup of the radiator testing and material identification.

8.1. Performance testing

As a consequence of the testing of the radiator, its performance was obtained. With this intention, the performance was measured through a correlation between the radiator's heat transfer and the internal fluid flow. Thus, dimensionless parameters for each physical phenomenon had to be defined. In this case, a correlation between the Nu number and Re for turbulent flow inside a tube, similar to the Colburn equation, which states an empirical relationship between both parameters:

$$Nu = A\, Re^{B} Pr^{1/3} \qquad \textbf{(Eq. 8.1)}$$

where *A* and *B* are unknown characteristic coefficients for this radiator (Çengel, 2006).

After evaluating those coefficients for a given Re numerical domain, the final mass flow rate found at the end of the design process could be applied in this correlation to find the Nu number and, therefore, find the heat exchange area needed through Eq. 4.7 and Eq. 4.3. In order to do that, eight different experiments were carried out: four different water mass flow rates for two different air velocities. As so, two total experimental correlations could be found and compared with each other.

8.1.1. Data collection and treatment

The heat exchanger was surrounded by thermal sensors which measured its temperature in different locations. These temperatures were measured by a data sensor, which sent the information to the computer and was presented with a software called *Data Studio*, shown in Figure 8.4.

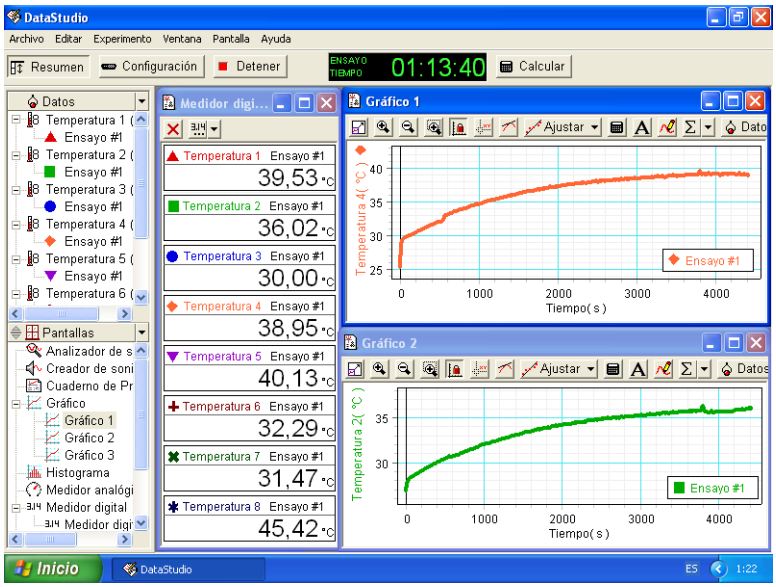

Figure 8.4 Screenshot of the software used to collect the radiator temperatures.

There were 8 sensors, measuring temperatures on the radiator surface, air temperatures and water temperatures. Although the needed ones were the inlet and outlets of the water temperature, the remaining data was to make sure the measurements were correct. Temperature data was read once a steady state was achieved. Then, all the data was saved and plotted in order to extract the needed information.

After that, all physical properties of water were calculated at the average temperature between the inlet and outlet. Secondly, with a previous measurement of the radiator – tubes thickness and fins dimensions – the internal Reynolds was calculated, as well as the convection heat transfer and Nusselt number. Finally, in order to find the correlation parameters – A and B – Eq. 8.1 was rewritten as:

$$\frac{Nu}{Pr^{1/3}} = A\, Re^{B} \qquad \textbf{(Eq. 8.2)}$$

In this way, it was necessary to plot $\frac{Nu}{Pr^{1/3}}$ against the Re number. This can be seen in Figure 8.5. for the two different air velocities – called V min and V max. In Figure 8.6 may be observed the total correlation of all the experiments with a straight power trend line, which also presented the equation that correlated the sought dimensionless numbers.

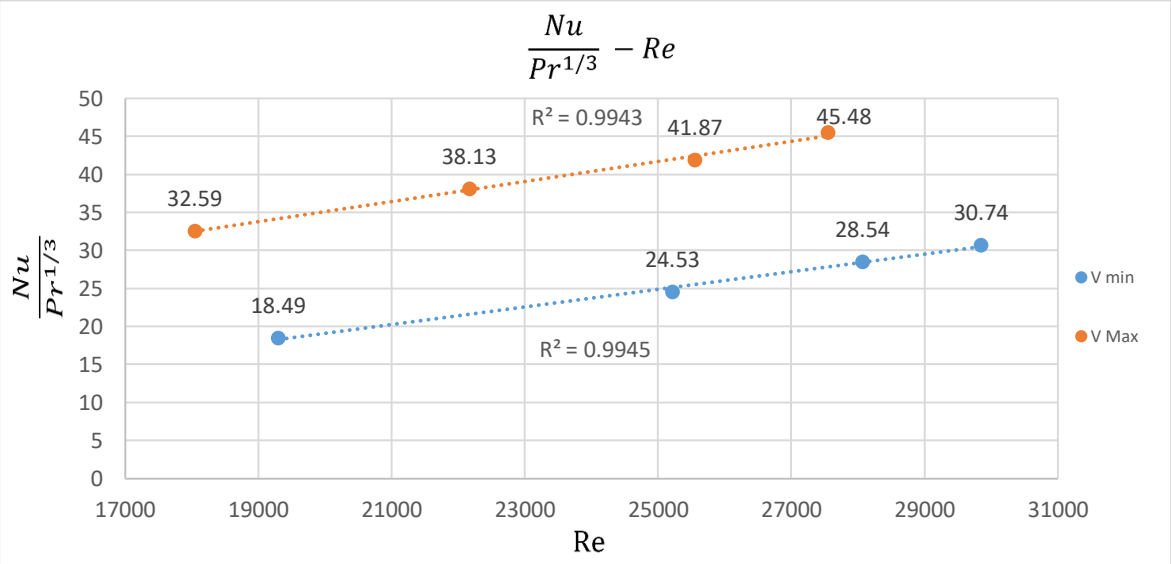

Figure 8.5 Plot representation of the two correlations obtained for each air velocity between the $\frac{Nu}{Pr^{1/3}}$ and the Re numbers.

It might be noticed the different values obtained for each air velocity, where V min stands for the minimum velocity the fan delivered and V max for its maximum one.

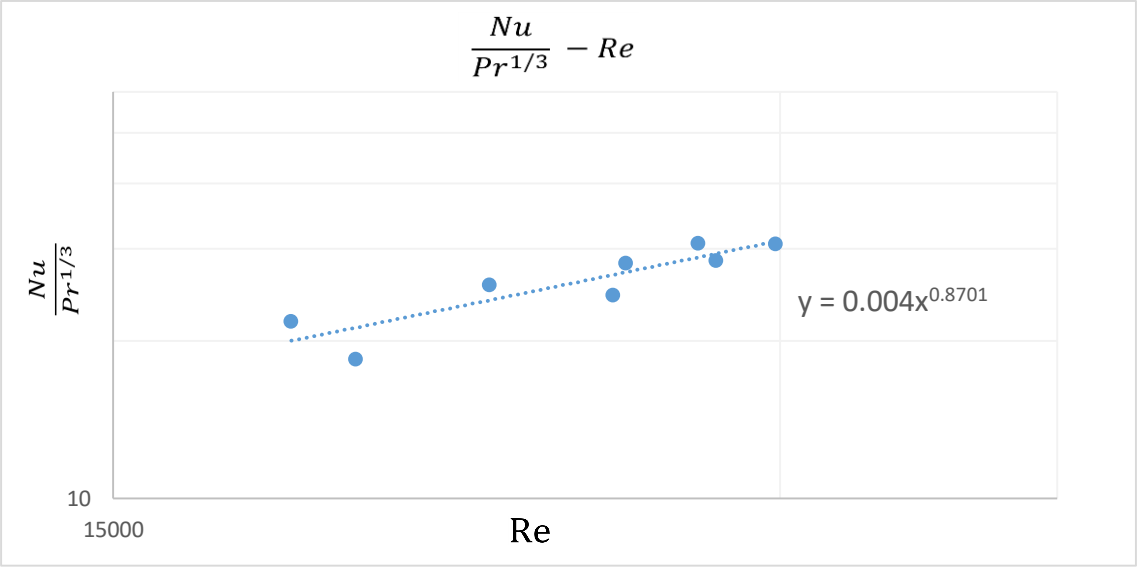

Figure 8.6 Correlation between the $\frac{Nu}{Pr^{1/3}}$ and the Re number in logarithmic scales. The equation represents the numerical correlation, valid for Reynolds from 19300 to 30000.

From Figure 8.6 it was extracted the trend line equation, which was

$$y = 0.004x^{0.8701} \quad \textbf{(Eq. 8.3)}$$

where parameters *A* and *B* could be deduced as 0.004 and 0.8701, respectively.

Finally, the final equation that described the internal heat transfer of the radiator in terms of its internal fluid velocity was:

$$Nu = 0.004Re^{0.8701}Pr^{1/3} \quad \textbf{(Eq. 8.4)}$$

With this equation, the remaining data needed to choose the heat exchange area was the water mass flow rate for the cooling system.

All the measurements and temperature plots can be found in Annex B.

9. Results

9.1. Preliminary simulation results

After performing the aforementioned numerical analysis, we obtained the first simulation results.

9.1.1. Cold Plate preliminary simulation results

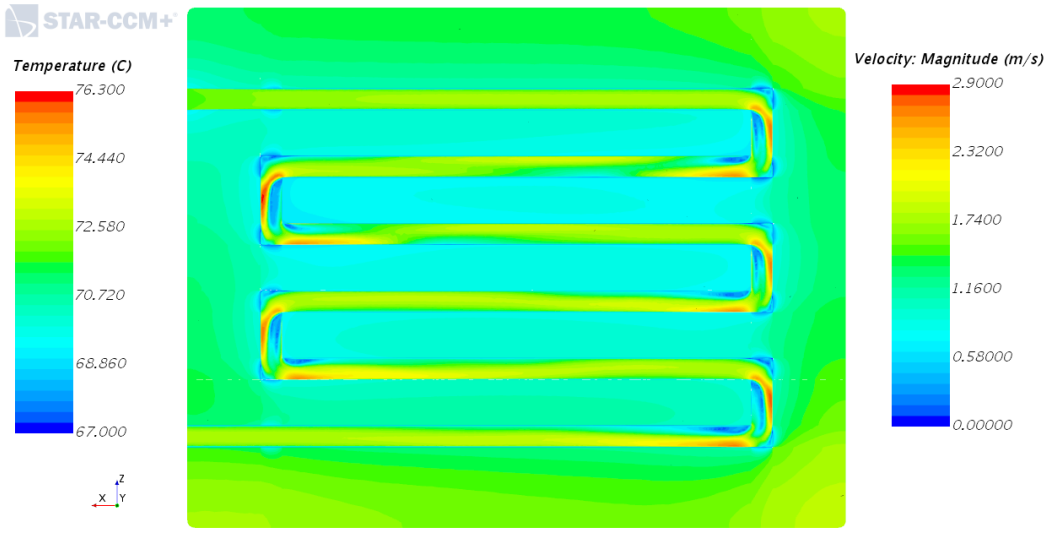

Figure 9.1 Representation of the drilled Cold Plate's temperature and fluid velocity in a cross-section plane.

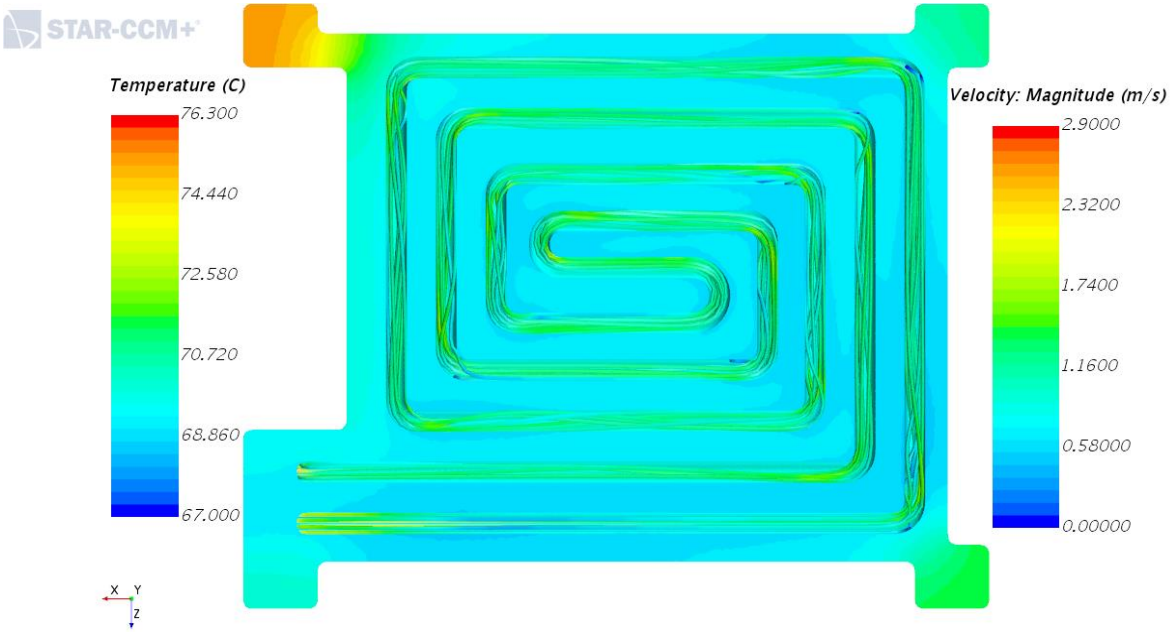

Figure 9.2 Representation of the machined Cold Plate's temperature and fluid velocity at 0.0412 kg/s.

As it was thought, the drilled Cold Plate resulted in a greater pressure drop than the machined one. However, the results were not such different from one to the other, as it might be seen in Table 9.1. The velocity differences appeared due to the characteristic diameter of the machined heat sink, which was 6.40mm alike the 6.00mm of the drilled one. The maximum temperatures were not important, since they were small spots of the heat exchanger which actually would not get that hot, as it can be seen in Figure 9.1 and Figure 9.2.

Config.	Pressure Drop (Pa)	T av. Heat Sink (ºC)	T max. Heat Sink (ºC)	T Max H2O (ºC)	T Outlet (ºC)	Average V (m/s)	Mass (Block) (g)
Drilled	16514	71.10	73.32	71.70	68.70	1.48	928
Machined	9132	70.37	76.30	70.50	68.65	1.06	749

Table 9.1 Simulation results for both Cold Plate models at a mass flow rate of 0.0412 kg/s.

9.1.2. Motor cooling block preliminary simulation results

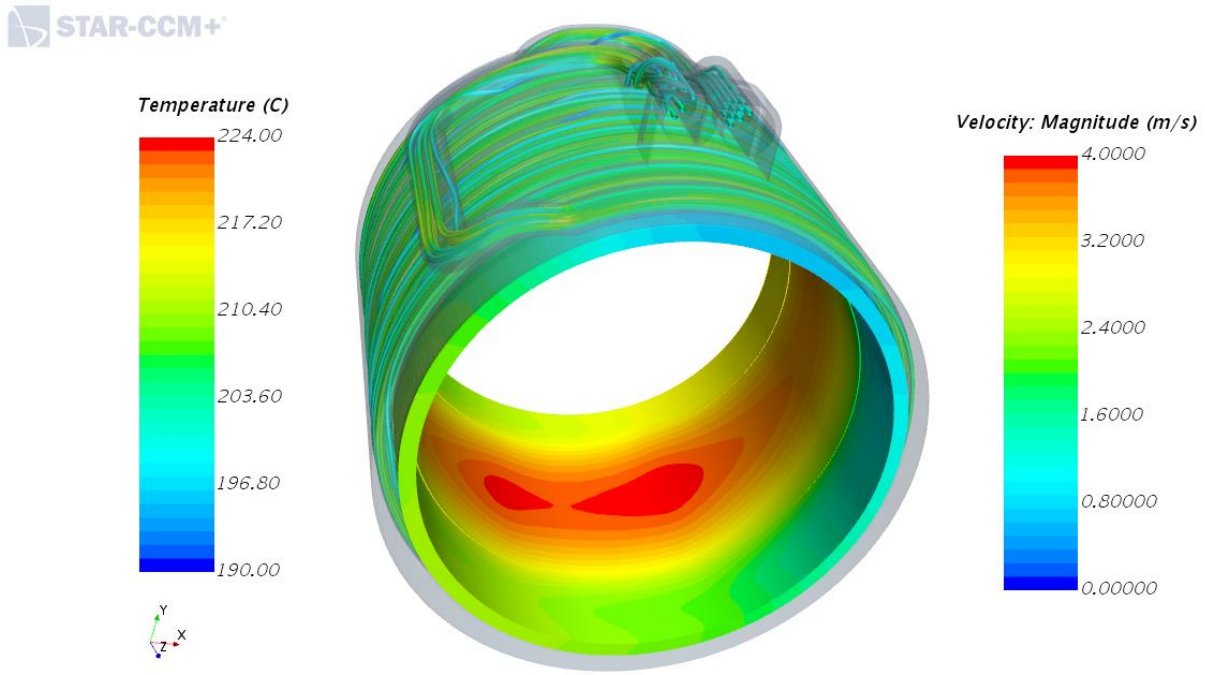

Figure 9.3 Representation of the C2 motor cooling block assembly's temperature and fluid velocity at 0.0412 kg/s.

As it was expected, the pressure drop increased as the water channel's profile area was reduced. Besides, the fluid velocity was lower than analytically calculated: the characteristic diameter was fairly different and, as it might be observed in the figures, it was not constant. The upper part of the water

channel had a different area than the heat exchange section – the one which surrounded the motor. Furthermore, the 3 revolutions models did not cover the whole cooling block, leading into very hot spots in the heat exchanger, as it is shown in Table 9.2.

However, the main problem found was the maximum temperature for the solids and fluid. For the 3 revolutions configurations the temperature reached was extremely high, making it completely unsuitable. The 8 revolution model achieved much lower temperatures, but still not enough to accomplish the main objective of not surpassing 135ºC on the inner face of the aluminium case. It can be noticed the heat losses distribution inside the motor in Figure 9.3.

Config.	Pressure Drop (Pa)	T Max Al (ºC)	T Max Nylon (ºC)	T Max H2O (ºC)	T Outlet (ºC)	Average V (m/s)	Mass (Block) (g)
A	5274	418.02	417.51	126.10	76.70	1.07	224
B	8131	411.11	411.03	113.42	75.20	1.31	176
C	13598	399.18	398.74	106.20	73.00	1.72	148
A2	9935	224.23	221.63	98.37	76.80	1.05	135
B2	14852	224.12	221.00	96.14	75.80	1.31	105
C2	29755	223.92	220.09	92.38	76.73	1.73	96

Table 9.2 Simulation results for the cooling block models at a mass flow rate of 0.0412 kg/s.

So, in order to check if there was another possibility for solving the temperature problem, a different mass flow rate was introduced, more specifically a flow rate of 0.0824 kg/s, the double amount that it was originally thought.

Therefore, the drilled Cold Plate was no longer suitable for this purpose, since such a mass flow rate would have induced into a fluid velocity much greater than 3 m/s, as it can be observed in Figure 9.1: every time the fluid changed its direction, its velocity was about 2.84 m/s. Opposite to the machined heat sink, where the water velocity was almost constant in all the channel except at the inlet and outlet, where the small change in the section induced maximum velocities of 2.80 m/s. Regarding the motor cooling block, the 3 revolution configurations were discarded.

9.2. Final simulation results

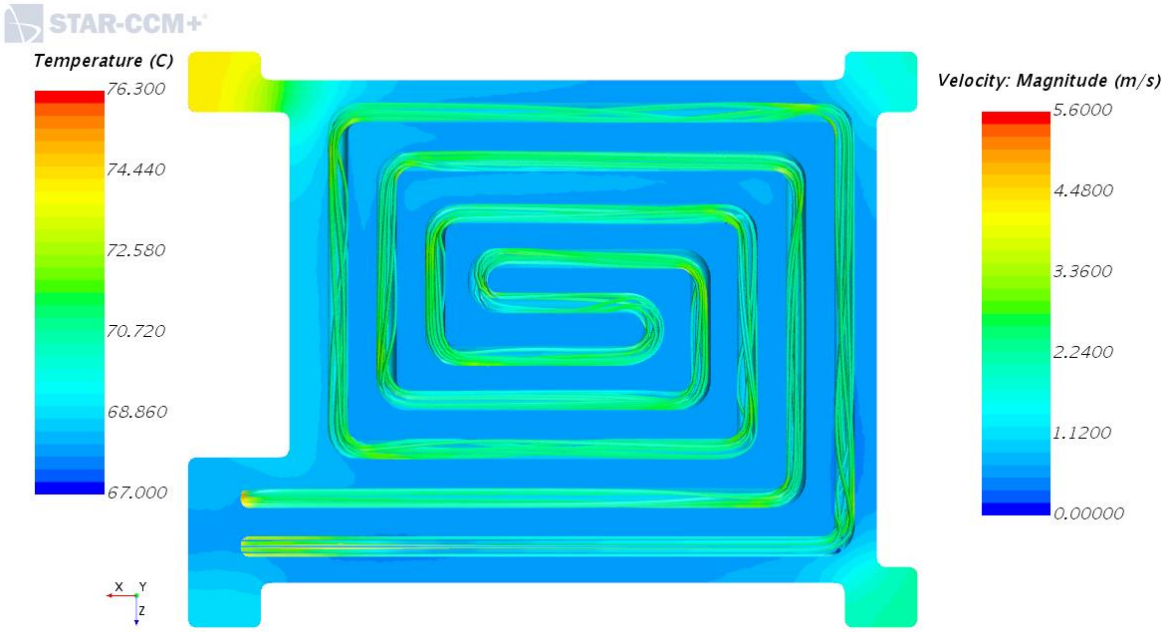

Figure 9.4 Representation of the machined Cold Plate's temperature and fluid velocity at 0.0824 kg/s.

The Cold Plate numerical analysis released a dramatic increase in pressure drop and a slight difference in temperatures, as it is represented in Figure 9.4. The results may in more detail at Table 9.3.

Config.	Pressure Drop (Pa)	T av. Heat Sink (ºC)	T max. Heat Sink (ºC)	T Max H2O (ºC)	T Outlet (ºC)	Average V (m/s)	Mass (Block) (g)
Machined	31800	69.30	75.14	69.26	67.88	2.12	749

Table 9.3 Simulation results for both Cold Plate models at a mass flow rate of 0.0824 kg/s.

Its outlet temperature served as the inlet temperature for the motor cooling block in the 8 revolutions configurations.

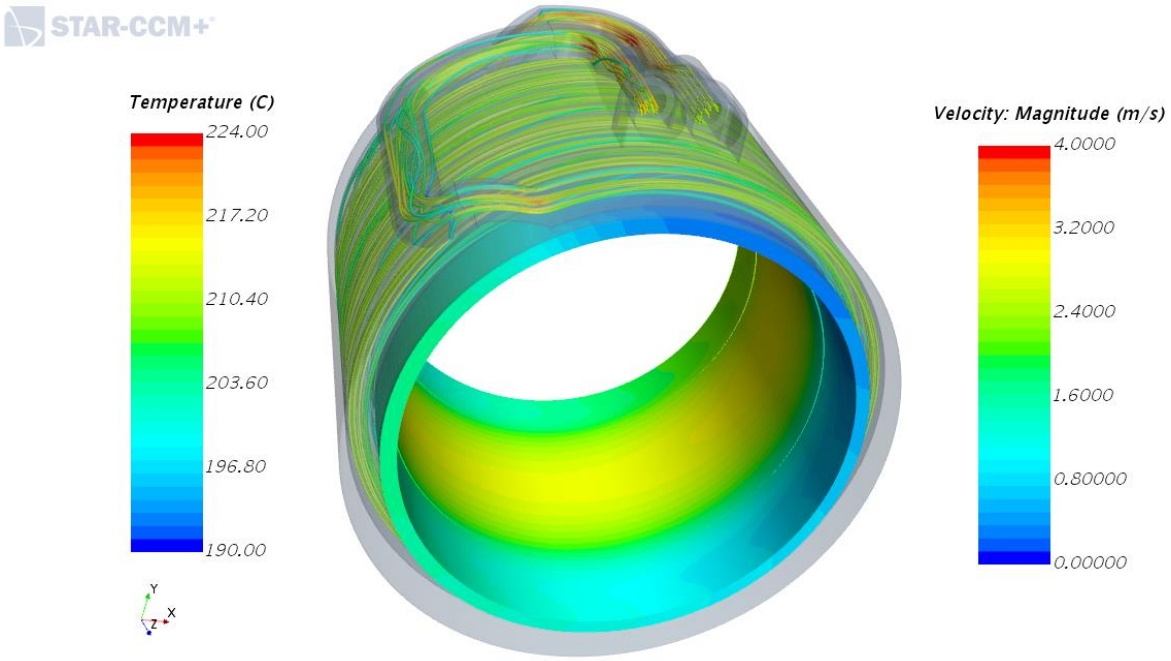

Figure 9.5 Representation of the A2 motor cooling block assembly's temperature and fluid velocity at 0.0824 kg/s.

A notable increase in pressure drop was also withdrawn from the motor cooling block's simulation. However, the maximum temperatures achieved on the aluminium case were really high, almost 100ºC above the objective requirement, shown in Figure 9.5. These results showed the incapability of a nylon cooling case as a heat exchanger for this application, since a double mass flow rate induced only a maximum decrease in the motor temperature of 8ºC, making this material unsuitable for this purpose, as it can be seen in Table 9.4.

Config.	Pressure Drop (Pa)	T Max Al (ºC)	T Max Nylon (ºC)	T Max H2O (ºC)	T Outlet (ºC)	Average V (m/s)	Mass (Block) (g)
A2	31800	215.92	213.41	85.88	74.45	2.10	135
B2	63140	217.57	214.02	85.20	74.94	3.18	105
C2	95000	218.32	214.36	84.94	75.22	3.46	96

Table 9.4 Simulation results for the cooling block models at a mass flow rate of 0.0824 kg/s.

Furthermore, the average velocity in configurations B2 and C2 were invalid, since they were greater than 3 m/s, leaving the only suitable cooling case the A2 configuration for the fluid velocity. Nevertheless, as it was stated in last paragraph, all cooling cases proposed for this project were discarded.

10. Environmental impact analysis

The environmental impact in this project has been so low that is has been decided not to include it in this project.

Conclusions

The conclusions obtained due to the final results of this project clearly indicate the unviability of this cooling system for an in-wheel motor powertrain system, primarily due to the material used for the motor cooling block. Since no water mass flow rate satisfied the required operating conditions, it has not been possible to accomplish the general objective of this project, which was selecting a cooling system – neither carrying out the pump selection, which was not included due to this impossibility.

On the one hand, both Cold Plate designs satisfied the thermal needs of the system in spite of the great pressure drop offered by the drilled heat sink. The temperature regions were quite homogeneous and the maximum temperature spots were the ones where water did not cross through, indicating a stable operating temperature range for the motor controllers. As so, both heat exchangers would work in a powertrain system of these characteristics.

On the contrary, the nylon motor cooling block did not fulfil the Formula Student team requirement of not surpassing 135ºC. Despite showing a homogeneous temperature region inside the aluminium case too, the temperature values were about 100ºC over the required value. This thermal homogeneity proves the effectiveness of the helix water channel around the motor. However, it has been observed that even large mass flow rates could not provide a safe range of temperatures, leading to the conclusion that nylon 3D printed heat exchangers are not suitable for such purposes.

For future works it is recommended to focus on the following aspects:

- Metal heat exchangers for the motor cooling – manufacturing analysis above all. More specifically, aluminium cooling blocks.
- To take into account the manufacturing costs for all self-designed heat exchangers.
- Keep studying CFD discretisation methods and numerical solvers.
- To think about the assembling options for the motor cooling block to the wheel. It is an inter-departmental task that is critical to the suspension, steering and brakes and wheels departments.

Budget analysis

The budget analysis, which is shown in Tables 1, 2 and 3, has been split up in three parts: the human resources budget, where all human resources expenses are analysed; an equipment cost analysis and a section chapter where all expenses are summarised.

It is important to notice that the calculated costs do not take into account the VAT.

Section 1: Human resources cost

It has been considered the participation of a junior engineer supervised by a senior engineer.

Personnel	Quantity	Unit cost	Cost
Junior engineer	600 hours	30 €/h*	18.000€
Senior engineer	40 hours	60 €/h*	2.400€
Total human resources cost			20.400€

Table 1. Summary of the human resources cost.

*This numbers are approximated values of the unit cost from the sponsorship to the Formula Student team.

Section 2: Equipment cost

It has been approximated a total of laptop working hours of 800h, taking 500h as numerical computation work. The cost is assigned for each nucleus of the laptop, in this case 4, according to a standard price stated by CSUC – ''*Consorci de Serveis Universitaris de Catalunya''*. Furthermore, it has been taken into account the cost of connecting the laptop to the grid: assuming an average power consumption of 70W and a use of 800h, results in an energy consumption of 56kWh. It is important to take into account the average price of electricity in Spain for 2018, which is 0.11€/kWh – according to Endesa.

The license cost of all software used has been chosen to be per hour, instead of showing the annual license price. Besides, the use of CAD software has been 200h, and the remaining 100h were MS Office.

On the other hand, the equipment used in the radiator testing has a cost, where the most expensive devices were the radiator and water pump – 71€ and 120€, respectively. Adding this to the other items - distilled water, plastic box and electronic devices – the sum is approximately 210€.

Concept	Quantity	Unit cost	Cost
Laptop simulation working hours	500 hours	0,05€/h x4 nucleus	100€
Laptop total working hours	800 hours	0.11€/kWh	88€
MS Office License 2016	1	0,022€/h	2,17€
SolidWorks 2016-2017 License	1	0,77€/h	77€
STAR-CCM+ License	1	1,194 €/h	716,50 €
Materials and resources to carry out the experimental radiator test	1	210€	210€
Total equipment cost			1.193,67€

Table 2. Summary of the equipment cost.

Section 3: Total cost

In this section is included the management of the project itself, which is estimated to be approximately the 15% of the total human resources cost plus the total equipment cost.

After computing the total cost of the project, there is also stipulated the commercial benefit of the project for the engineers.

Concept	Cost
Human resources	20.400€
Equipment	1.193,67€
Administrative cost	3.239.05€
Without VAT	24.832,72€
VAT 21%	5.241,87€
Total cost of the project	30.074,59€
Commercial benefit	13.958,59€

Table 3. Total cost of the project and commercial benefit, split up in sections.

Bibliography

Aune, Peder August. 2016. *A Four Wheel Drive System for a Formula Style Electric Racecar*, no. February.

Bakker, André. 2006. *Lecture 1 - Introduction to CFD Applied Computational Fluid Dynamics*. *Fluid Dynamics*, no. 2002: 1–36.

Cengel YA. 2007. *Heat and Mass Transfer A Practical Approach*. McGraw-Hill, Mexico.

Elmo Motion Control Ltd. (2018). *GOLD DRUM HV Physical Specifications 800V Type.* [Consulted 13th February 2018]. Available at: <https://www.elmomc.com/product/gold-drum-hv-100-a800-v/>

Formula Student Germany. (2018). *Formula Student Rules 2018*. [Consulted 22nd February 2018]. Available at: <https://www.formulastudent.de/fileadmin/user_upload/all/2018/rules/FS-Rules_2018_V1.1.pdf>

Hooper, Ian. 2011. *Development of in-wheel motor systems for Formula SAE electric vehicles*. The University of Western Australia.

MakeItFrom: Material Properties Database [Consulted 15th September 2018]. Available at: < https://www.makeitfrom.com/>

Menter, F.R. 1994. *Two-equation eddy-viscosity turbulence modelling for engineering applications*, AIAA Journal, 32(8), pp. 1598-1605.

Setrab (2018). Setrab Proline STD Oil-Coolers. [Consulted 21st February 2018]. Available at: <http://www.setrab.com/products/proline/products/std-oil-cooler/>

SIEMENS (2018). *STAR-CCM+ Documentation*. [Consulted 25th February 2018]. Available at: <https://documentation.thesteveportal.plm.automation.siemens.com/starccmplus_latest_en/index.html?param=Wlxl0&authLoc=https://thesteveportal.plm.automation.siemens.com/AuthoriseRedirect>

SimScale CAE Forum (2018). *What is y+ (yplus)?* [Consulted 15th May 2018]. Available at: <https://www.simscale.com/forum/t/what-is-y-yplus/82394/1>

Styger, Erich (2014). *Formula Student Electric "grimsel'' Testing in Alpnach.* [Consulted 29th April 2018]. Available at: < https://mcuoneclipse.com/2014/06/22/formula-student-electric-grimsel-testing-in-alpnach/>

Torrents, Bernat. 2018. *Estudio y diseño de la refrigeración de un motor eléctrico para una monoplaza de Formula Student*

Unitek Gmbh. (2018). Digital three-phase Servo Amplifier BAMOCAR-PG-D3 Manual V 02. [Consulted 13th February 2018]. Available at: <https://www.unitek-industrie-elektronik.de/images/pdf/BAMOCAR%20Digital/BAMOCAR-PG-D3_EN.pdf>

Versteeg H. K. and Malalasekera W. 2007. *An Introduction to Computational Fluid Dynamics: The Finite Volume.* Pearson Prentice Hall, England.

White, Frank. 2010. *Fluid Mechanics*. McGraw-Hill,New York.

Wilcox, D.C. 1988. *Turbulence Modelling for CFD*, 2nd edition, DCW Industries, Inc.

Annex A. Datasheet of the cooling block's nylon.

B.Sc. DISSERTATION

Bachelor's degree in Mechanical Engineering

DESIGN OF A COOLING SYSTEM OF AN ELECTRIC FORMULA STUDENT CAR

Annex A

Author: Luis Alberto Castrillo Jiménez
Director: Alfredo Guardo Zabaleta

Summons: October 2018

A1. Technical specifications of the HP 3D High Reusability PA 12 Glass Beads

Category	Measurement	Value	Method
General properties	Powder melting point (DSC)	186 °C/367 °F	ASTM D3418
	Particle size	58 µm	ASTM D3451
	Bulk density of powder	0.48 g/cm3/0.017 lb/in3	ASTM D1895
	Density of parts	1.3 g/cm3/0.047 lb/in3	ASTM D792
Mechanical properties	Tensile strength, max load7, XY, XZ, YX, YZ	30 MPa/4351 psi	ASTM D638
	Tensile strength, max load7, ZX, XY	30 MPa/4351 psi	ASTM D638
	Tensile modulus7, XY, XZ, YX, YZ	2500 MPa/363 ksi	ASTM D638
	Tensile modulus7, ZX, XY	2700 MPa/392 ksi	ASTM D638
	Elongation at break7, XY, XZ, YX, YZ	10%	ASTM D638
	Elongation at break7, ZX, XY	10%	ASTM D638
	Flexural strength (@ 5%),8 XY, XZ, YX, YZ	57.5 MPa/8340 psi	ASTM D790
	Flexural strength (@ 5%),8 ZX, XY	65 MPa/9427 psi	ASTM D790
	Flexural modulus,8 XY, XZ, YX, YZ	2400 MPa/348 ksi	ASTM D790
	Flexural modulus,8 ZX, XY	2700 MPa/392 ksi	ASTM D790
	Izod impact notched (@ 3.2 mm, 23ºC), XY, XZ, YX, YZ, ZX, ZY	3 KJ/m2	ASTM D256 Test Method A
	Shore Hardness D, XY, XZ, YX, YZ, ZX, ZY	82	ASTM D2240
Thermal properties	Heat deflection temperature (@ 0.45 MPa, 66 psi), XY, XZ, YX, YZ	174 °C/345 °F	ASTM D648 Test Method A
	Heat deflection temperature (@ 0.45 MPa, 66 psi), ZX, XY	175 °C/347 °F	ASTM D648 Test Method A
	Heat deflection temperature (@ 1.82 MPa, 264 psi), XY, XZ, YX, YZ	114 °C/237 °F	ASTM D648 Test Method A
	Heat deflection temperature (@ 1.82 MPa, 264 psi), ZX, XY	120 °C/248 °F	ASTM D648 Test Method A
Reusability	Refresh ratio for stable performance	30%	
Recommended environmental conditions	Recommended relative humidity	50-70% RH	
Certifications	UL 94, UL 746A		

Annex B. Radiator measurements and temperature plots.

B.Sc. DISSERTATION

Bachelor's degree in Mechanical Engineering

DESIGN OF A COOLING SYSTEM OF AN ELECTRIC FORMULA STUDENT CAR

Annex B

Author: Luis Alberto Castrillo Jiménez
Director: Alfredo Guardo Zabaleta

Summons: October 2018

B1. Measurements and plots

	Time (s)			
Measure number	**5V**	**4V**	**3.5V**	**3V**
1	5.85	6.38	7.12	8.78
2	5.90	6.40	7.31	8.72
3	6.00	6.21	7.13	8.71
4	5.90	6.31	7.34	8.93
5	6.00	6.22	7.16	8.88
Average time	5.93	6.30	7.21	8.80
LPM	**20.23**	**19.04**	**16.64**	**13.64**

Table 1. Volumetric flow rate measurement for the different pump input voltages.

	Measure 1	Measure 2	Measure 3	Measure 4	Measure 5	Average
V min (m/s)	1.73	1.88	1.74	1.76	1.79	**1.78**
V max (m/s)	2.18	2.30	2.19	2.15	2.12	**2.18**

Table 2. Air velocities measured with the anemometer at the outlet of the radiator.

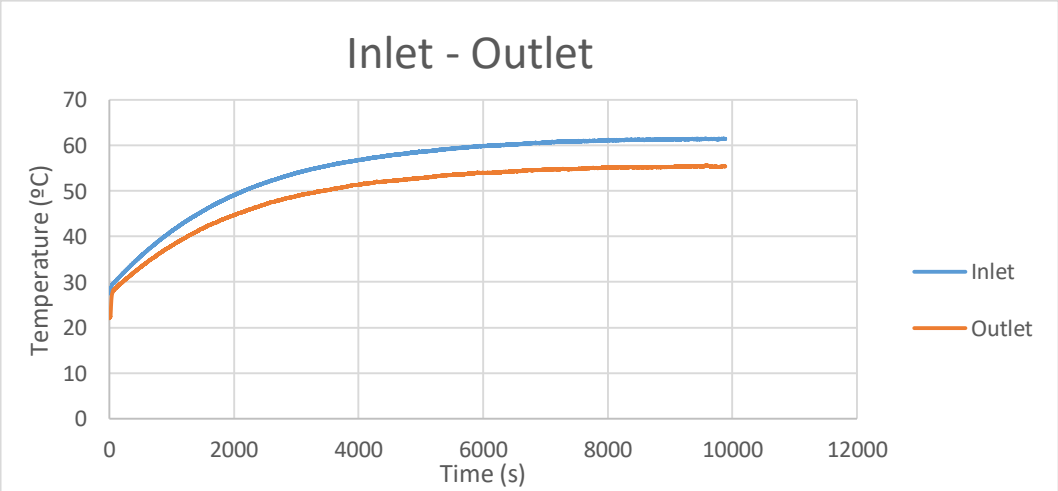

Figure 1. Water temperatures for a volumetric flow rate of 13.64 LPM at minimum fan velocity.

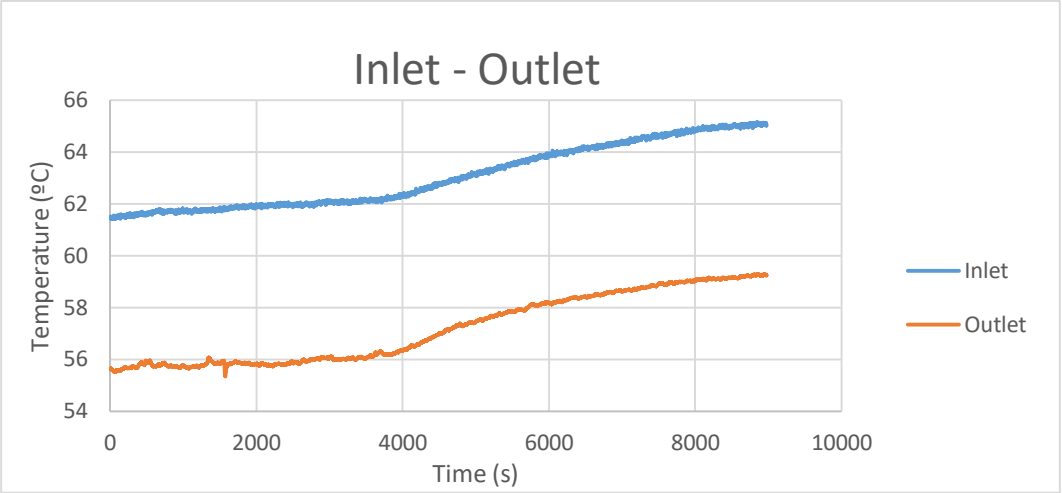

Figure 2. Water temperatures for a volumetric flow rate of 16.64 LPM at minimum fan velocity.

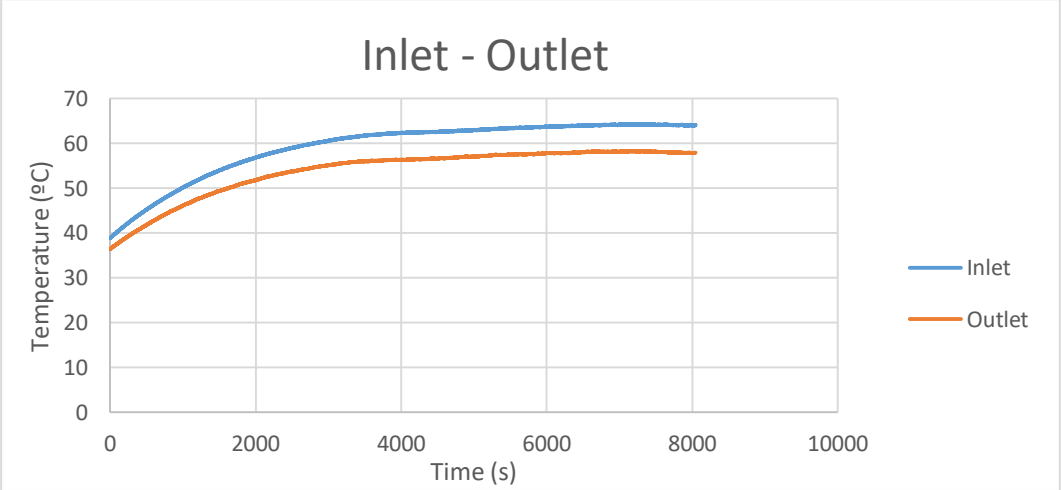

Figure 3. Water temperatures for a volumetric flow rate of 19.04 LPM at minimum fan velocity

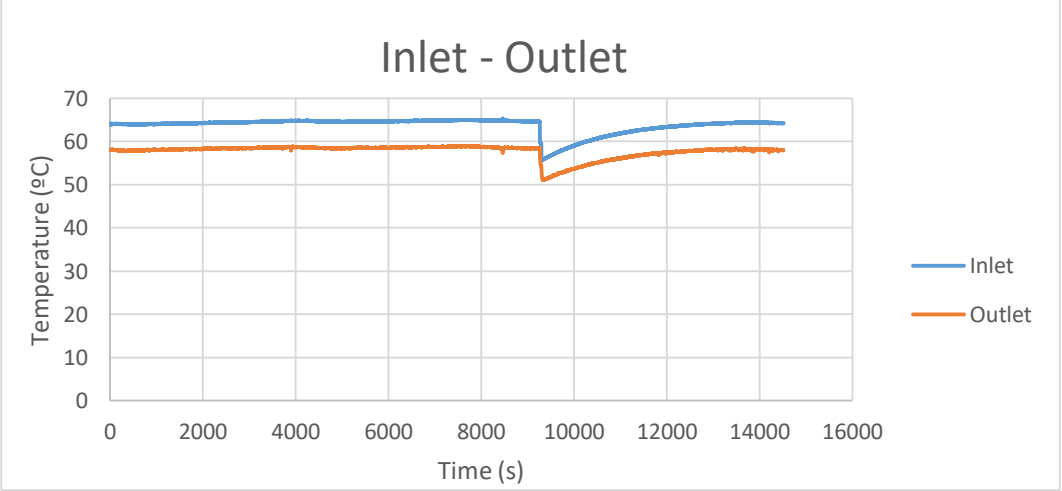

Figure 4. Water temperatures for a volumetric flow rate of 20.23 LPM at minimum fan velocity

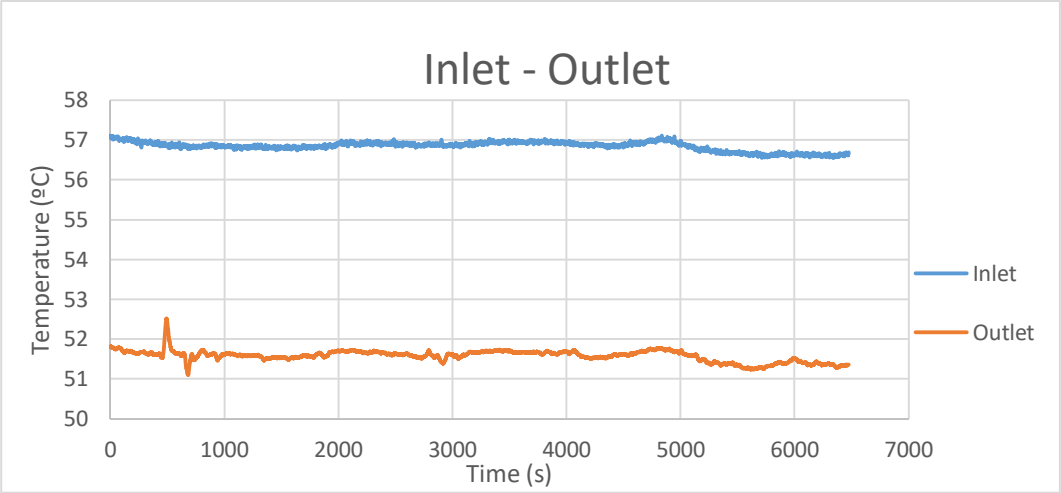

Figure 5. Water temperatures for a volumetric flow rate of 13.64 LPM at maximum fan velocity.

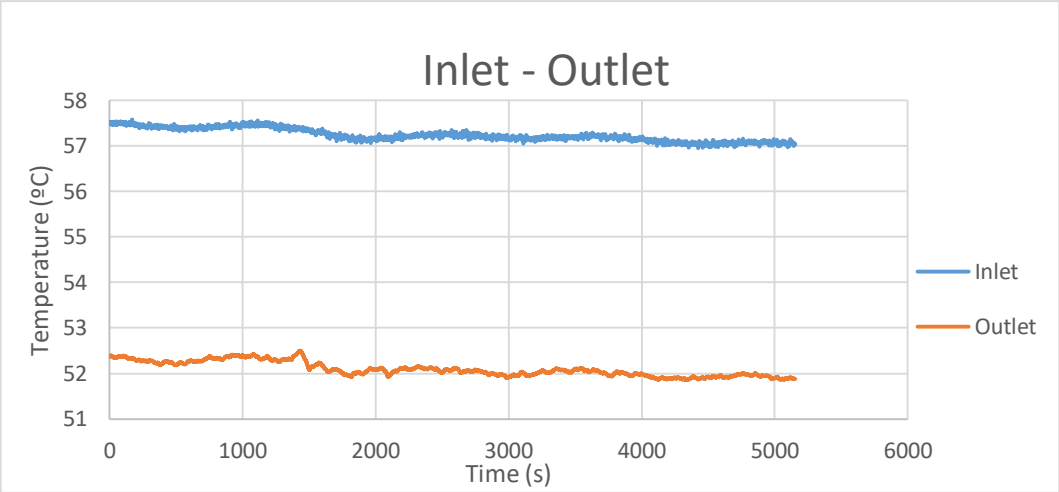

Figure 6. Water temperatures for a volumetric flow rate of 16.64 LPM at maximum fan velocity.

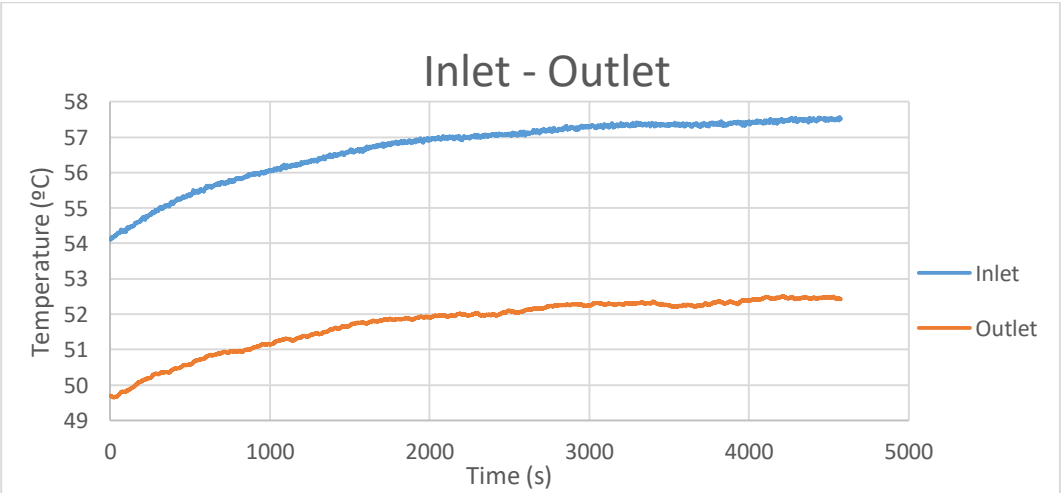

Figure 7. Water temperatures for a volumetric flow rate of 19.04 LPM at maximum fan velocity.

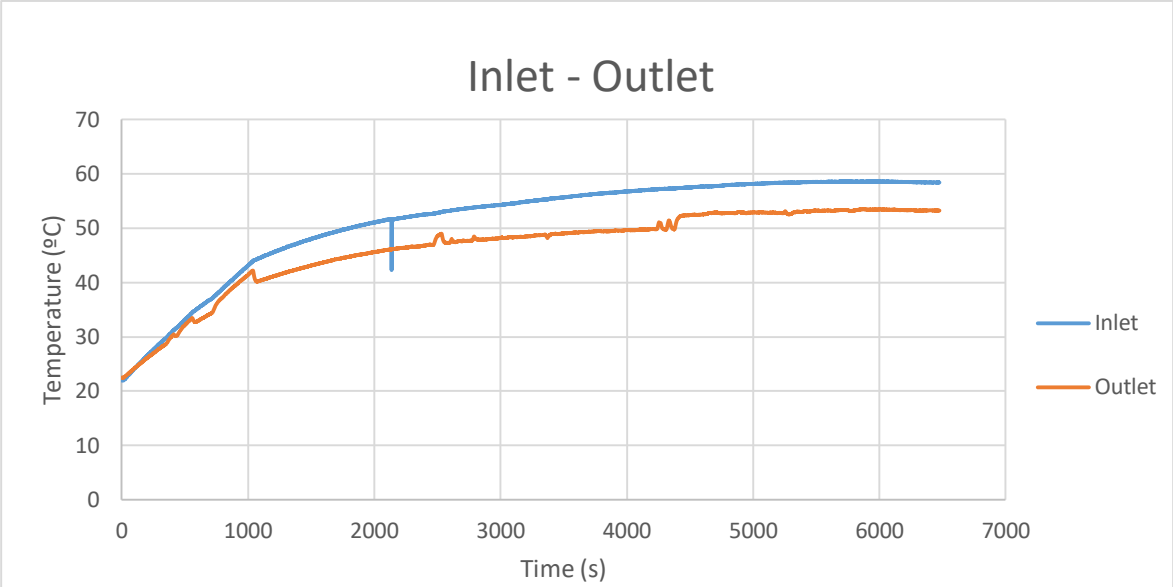

Figure 8. Water temperatures for a volumetric flow rate of 20.23 LPM at maximum fan velocity.